

Gas hydrate destabilization and methane release events in the Krishna-Godavari basin, Bay of Bengal

R. K. Joshi¹, A. Mazumdar^{2,*}, A. Peketi³, P. B. Ramamurty⁴, B. G. Naik², M. Kocherla², Mary Ann Carvalho², P. Mahalakshmi², P. Dewangan² and M. V. Ramana²

¹Geological Survey of India
Kolkata-700 091, India

²CSIR-National Institute of Oceanography
Dona Paula, Goa-403 004, India
**maninda@nio.org (corresponding)*

³Physical Research Laboratory,
Ahmedabad, Gujarat-3800 09, India

⁴National Geophysical Research Institute
Uppal Road, Hyderabad-500 606, Andhra Pradesh, India

Abstract

Methane release events have been linked to global warming, alteration of the carbon cycle and influence on biota. However, unequivocal evidence of paleomethane release events are limited. We report several negative carbon stable isotope excursions in planktic and benthic foraminifera in a core (MD161-8) from the Krishna-Godavari (K-G) Basin, Bay of Bengal. The most negative $\delta^{13}\text{C}$ spikes are recorded during the marine isotope stages MIS-4 and at the transition of MIS-5 to 4. Occurrence of highly ^{13}C depleted (average $\delta^{13}\text{C} = -48 \pm 2.4$ ‰ VPDB) authigenic high magnesian calcite are also reported within this time window from the core MD161-8. In the present work an unequivocal explanation for the observed ^{13}C depletion in the marine planktic and benthic foraminifera is difficult to achieve solely from the optical/electron microscopy or C-O stable isotope ratio analyses due to possible influence of diagenetic alteration. We attribute the observed episodic methane expulsion events, as inferred from the negative $\delta^{13}\text{C}$ excursions and earlier reports on the occurrence chemosynthetic bivalves and Mo concentration anomaly to the destabilization of the base of gas hydrate stability zone (BGHSZ). Sea level drop and shale tectonics induced focused fluid flow are the two possible causes of hydrate destabilization discussed here. Shale tectonics were possibly responsible for creating fault systems which acted as the conduit for gas flow through the sediment column and subsequent seepage. Shale and salt tectonics in the passive continental margins being a globally observed phenomenon, its role as an important driving force for enhanced methane emission needs detailed investigation to understand the climatic perturbations through geologic time. Additional evidence of methane emission from site MD161-15 further supports the link between shale tectonics and methane emission.

Key words: methane emission, gas hydrate, shale tectonics, carbon isotope, oxygen isotope, passive margin

1. Introduction

Perturbation in methane concentrations in the ocean-atmosphere system may cause global warming (Lashof and Ahuja, 1990) and alteration of the carbon cycle (Dickens, 2003). Vast reserves of methane hydrate, a crystalline form of methane-water complex (molar ratio 1:6) exist within the marine sediments at suitable temperature-pressure conditions subject to the availability of methane in excess of solubility (Kvenvolden, 1993; Sloan, 1998; Kvenvolden and Lorenson, 2001). Whereas, methane from shallow sub-seafloor (Hovland and Judd, 1992; Mazumdar et al., 2009a; Coffin et al., 2013) are additional sources of marine methane to the global budget. The terrestrial sources influencing the global methane budget include volcanic eruptions, natural wetlands, rice and paddy fields, enteric fermentation, coal mining, biomass burning, soil microseepage, geothermal activity (Chanton and Whiting, 1996; Judd et al., 2002; Kaplan, 2002; Etiope et al., 2008; Sanchez Goni et al., 2008) and ebullition from thermokarst lakes (Walter et al., 2006). Carbon stable isotope ratios of foraminifera (Kennett and Stott, 1991; Kennett et al., 2000; Kennett et al., 2003; De Garidel-Thoron et al., 2004; Hill et al., 2004a; Uchida et al., 2004; Cook et al., 2011) as well as measurement of methane concentrations in the Greenland and Antarctic ice deposits (Chappellaz et al., 1997; Dällenbach et al., 2000; Wolf and Spahni, 2007) suggest repeated enrichment of methane concentrations in the ocean-atmosphere system. Methane enrichment has primarily been attributed to the hydrate destabilization due to increase in marine bottom water temperature during interstadials (Kennett et al., 2003; De Gadriel-Thoron et al., 2004), depressurization from lowering of sea level or slope failure (Buffett and Archer, 2004; Archer, 2007).

Marked enrichment in methane concentrations in ancient water column/ atmosphere has been inferred from the late Neoproterozoic (Kennedy et al., 2008), early Jurassic (Kemp et al., 2005), early Cretaceous (Jahren et al., 2001), Paleocene-Eocene (Dickens et al., 1995), Miocene (Panieri et al., 2009) and late Quaternary (Kennett et al., 2000; Hinrichs et al., 2003; De-Gadriel-Thoron et al., 2004). Methane enrichment episodes prior to Preboreal-Younger Dryas transition has primarily been attributed to methane hydrate destabilization (Kennett et al., 2003). In contrast, δD_{CH_4} (Sowers, 2006; Bock et al., 2010) and $^{14}CH_4$ (Petrenko et al., 2009) data from ice cores, suggest that marine methane hydrate degassing may not be the cause of atmospheric methane enrichment intervals through late Quaternary. Although, a significant volume of work (Wefer et al., 1994; Kennett et al., 2000; Smith et al., 2001; Hill et al., 2003; Kennett et al., 2003; De-Gadriel-Thoron et al., 2004; Panieri et al., 2012; Wang et al., 2013) correlate ^{13}C depletion in planktic and benthic foraminifera to ^{13}C depleted bicarbonate ion produced via

aerobic/ anaerobic oxidation of methane in water column/ sediment-water interface, a significant number of publications attribute the ^{13}C depletion to diagenetic alteration of non-living foraminifera (Martin et al., 2004; Ohkushi et al., 2005; Wiedicke and Weiss, 2006; Uchida et al., 2008; Torres et al., 2010 and Cook et al., 2011; Herguera et al., 2014). Diagenesis results in precipitation of authigenic carbonate into the shell cavities or recrystallisation of shell ultrastructure. The controversy regarding the ^{13}C depletion in foraminifera and latter's association with methane emission is primarily due to the lack of routine/ rapid methods for unequivocal selection of unaltered foraminifera shells. It is also difficult to understand cryptic alterations in apparently clean shells which may result in significant ^{13}C depletion.

We present here, carbon-oxygen stable isotope ratios of planktic and benthic foraminifera and carbon isotope ratios of sediment organic matter and lipid extracts in a sediment core (MD161-8) from the Krishna-Godavari (K-G) Basin, Bay of Bengal (Fig. 1). Recently, paleo-cold seepage associated authigenic carbonate and chemosynthetic clam (*Calypptogena sp.*) shells have been reported from this site (Mazumdar et al., 2009b and 2011) and nearby site NGHP-10D (Collett et al., 2008). Based on ^{14}C and U/Th age dating of foraminiferal tests and authigenic carbonates respectively, a minimum age of 46 to 58 kyr was suggested for the methane expulsion events (Mazumdar et al., 2009).

In this work we have investigated the possible influence of methane emission on carbon isotope ratio of planktic and benthic foraminifera and further constrained the ages of the major methane expulsion events. We have also discussed the significance of shale tectonics as a possible mechanism to trigger methane release from the sediments of K-G basin. Additional evidence of shale tectonics induced methane expulsion and authigenic carbonate precipitation are presented from another coring location (MD161-15) in K-G basin. Our study locations lie within the continental slope region of eastern India (Fig. 1).

2. Geological Setting

The Krishna-Godavari basin is a passive margin, pericratonic rift basin located in the central part of the eastern continental margin of India, covering an area of 28,000 km² on land and 145,000 km² offshore. It has a maximum sediment thickness of ~8 km in the offshore region. The Krishna and Godavari rivers supply the bulk of the detrital sediments in to the basin. Smectite bearing Godavari Clay Formation constitutes the Holocene-Pleistocene deposit of the K-G basin (Rao, 2001). The seismic reflection data off K-G basin (Collett et al., 2008; Dewangan et al., 2010; Shankar and Riedel, 2010)

show regional presence of gas hydrates manifested in the form of bottom simulating reflectors (BSR) observed at depth of 125 mbsf (water depth: 945m) to 220 mbsf (water depth 1146 m). BSRs represent a phase boundary, where the low-velocity, gas-charged sediments occur below the high-velocity gas hydrate bearing sediments (Singh and Minshull, 1993). Ramana et al. (2007) and Dewangan et al. (2010) have reported various shale tectonics induced structures like bathymetric mounds, deep seated shale diapirs and toe thrust faults from the K-G basin. Both coring sites (MD161-8 and 15) are located on the top of bathymetric mounds. These bathymetric mounds are commonly associated with fluid/gas migration features and show numerous fault systems which facilitate the flow and accumulation of gas hydrate (Dewangan et al., 2011).

3. Methods

Two piston cores of lengths 30 m (MD161-8: Lat. =15° 51.8624'N and Long. = 81° 50.0692'E) and 31 m (MD161-15: Lat. =16° 00.5700' N and Long. = 82° 03.4502' E) were collected on-board *Marion Dufresne* (MD-161: May, 2007) using a Giant Calypso piston corer at water depths of 1033 and 983m respectively (Fig. 1). Close to the site MD161-8, sea water temperature and salinity profiles (Suppl. Figure-1) were generated using CTD system SBE 911plus (Seabird electronics ltd. USA). SEASOFT software modules have been used to calibrate and process the data from various sensors. The BGHSZ is calculated using an excel program based on linear approximation of the Maekawa et al. (1995) polynomial equation for CH₄ hydrate P-T stability in water of 3.5% NaCl salinity (Tim Collett, *personal correspondence*). A geothermal gradient of 44°C/km has been reported by Collett et al.(2008) for the NGHP site 10D near to our coring location (MD161-8) in the K-G basin.

Gamma density (wet bulk density) of the whole cores was measured on board using a GEOTEK Multisensor Core Logger (MSCL) following standard GEOTEK calibration and measurement protocol. Assuming that the sediment is fully saturated with water and the grain and fluid densities are known, the porosity (ϕ), wet bulk density (ρ_{MSCL}), grain density ($\rho_s = 2.65$ g/cc) and fluid density ($\rho_{fl} = 1.03$ g/cc) can be linked by equation-1. Porosity data is from Mazumdar et al.(2009)

$$\rho_{MSCL} = \phi\rho_{fl} + (1 - \phi)\rho_s \quad (\text{Eq. 1})$$

Grain size analyses was carried out using a Microtrac Tri-Laser S3500 laser particle size analyzer of Metrohm. It uses 780 nm laser beams and has an assembly of 151 detector arranged in 0.02

to 163° curve. Prior to sampling, the sediment samples were desalinated and subsequently decarbonated using dilute HCl (1N). Organic carbon was removed by 10 % v/v H₂O₂. Na-hexametaphosphate was added to the final suspension to ensure decoagulation in the flow path of the suspension. Online ultrasonication was used in the particle flow path. The grain size values are reported as volume %.

Dried and weighed aliquots of the sediment samples (MD161-8) were suspended in distilled water and gently sieved through 63 µm mesh sieve. Approximately 10 to 15 clean tests of *Globigerinoides ruber* (*G. ruber*: planktic) and *Uvigerina* sp. (benthic) with the size ranging from 250-355 µm were picked from the oven dried >63 µm fraction for oxygen and carbon stable isotope ratio measurement. Prior to the analyses, the foraminiferal tests were broken, cleaned in 5-10% H₂O₂ and followed by ultrasonication in distilled water and methanol to remove contaminants. An aliquot from each sample was examined under scanning electron microscope (JEOL JSM-5800LV) for signs of dissolution and recrystallization. The images are taken in both normal and backscatter mode. Samples for oxygen and carbon stable isotope ratios were analyzed in a Kiel III carbonate preparation device interfaced with a Finnigan-MAT 252 isotope ratio mass spectrometer at the Department of Geological Sciences, University of Florida. This is a dual inlet system having a precision of 0.04 ‰ VPDB for δ¹³C and 0.08 ‰ VPDB for δ¹⁸O for calcite standard NBS-19.

Carbon isotope measurement of total organic carbon were carried out using a Thermo-Finnigan Delta-V-Plus continuous flow isotope ratio mass spectrometer attached to an elemental analyzer (Thermo EA1112). The external precision calculated for δ¹³C is typically 0.07–0.09 ‰ (VPDB). Carbon isotope ratios are reported in standard format relative to VPDB standard. Total inorganic carbon (TIC) content was determined by carbon coulometer (UIC–CM5130). Total carbon (TC) content was measured by elemental analyzer (Thermo EA1112). Total organic carbon (TOC) was calculated by subtracting TIC from TC. Ultrapure CaCO₃ (Sigma-Aldrich) was used as standard for TIC measurement. Precision for TC and TIC measurements are 1 and 1.4% respectively.

AMS ¹⁴C dates for one core (MD161-15) were generated at the National Ocean Sciences AMS (NOSAMS) facility, Woods Hole Oceanographic Institution, USA. Dates were determined on planktic foraminifera. Carbon dioxide generated from these foraminifera shells was reacted with catalyst to form graphite which was pressed into targets and analyzed on the accelerator along with standards and

process blanks. Two primary standards used during ^{14}C measurements are NBS Oxalic Acid I (NIST-SRM-4990) and Oxalic Acid II (NIST-SRM-4990C).

Authigenic carbonate precipitates and shell fragments in MD161-15 were isolated, cleaned and photographed. Mineralogical identification was carried out using a Rigaku X-ray diffractometer (Ultima-IV). All the carbonate samples were run from 25 to 32° 2 θ at 1°/min scan speed using $\text{CuK}\alpha$ radiation ($\lambda = 1.541838\text{\AA}$). The MgCO_3 (mole %) was calculated using a MgCO_3 (mole %) d-spacing standard curve in Hardy and Tucker (1988). Carbon and oxygen isotope ratios of four authigenic carbonate samples from MD161-15 were determined with a Thermo Delta V continuous flow isotope ratio mass spectrometer attached with a GASBENCH II and equipped with a PAL auto sampler at the National Geophysical Research Institute, Hyderabad, India. The carbon isotope ratios are reported in standard $\delta^{13}\text{C}$ and $\delta^{18}\text{O}$ format relative to VPDB standard. A sample reproducibility of 0.1‰ for both carbon and oxygen is reported here.

For total lipid extraction, 15g of freeze dried and pulverized sediment aliquots from MD161-8 were extracted with a mixture of CH_2Cl_2 : CH_3OH (1:1, vv) three times using ultrasonication for 15 minutes. Extracts were desulfurized with activated copper and vacuum evaporated to near dryness, and hydrolyzed (saponification) overnight with 15ml of 10% KOH in methanol. Non-saponifiable compounds were recovered with hexane/diethyl ether (9:1) mixture (4X20ml). The resultant extract is concentrated to 1 ml and eluted through a liquid chromatography column (20 X 0.8 cm) filled with 4.2g of silica gel (60-120 mesh) deactivated with 5% water by weight. The three fractions, namely aliphatic hydrocarbons, aromatic and alcohols, were eluted sequentially with the 40 ml n-hexane, 32 ml n-hexane plus 8 ml toluene and 32 ml n-hexane plus 8 ml ethyl acetate respectively. The aliphatic fractions were reduced to 800 μl for GC/MS analysis. Perdeuterated Docosane ($\text{C}_{12}\text{D}_{26}$, 0.8 μg) was added as an internal standard. GC-MS was performed using a Shimadzu QP-2010 gas chromatograph interfaced with a QP2010 mass spectrometer. The gas chromatograph is equipped with a 30 m long Rtx-5 MS capillary column from Restek, USA.

Compound specific $\delta^{13}\text{C}$ values of the aliphatic hydrocarbon fraction were determined using a Thermo delta V plus isotope ratio mass spectrometer coupled with a Thermo Trace GC. A DB5 (length: 30m, ID = 0.25 mm, film thickness = 0.25 μm) column was used for chromatographic separation of compounds. Separated compounds are sequentially carried by the helium into the GC combustion unit at

980°C. CO₂ produced through combustion is subjected to isotope ratio measurement. δ¹³C values are given in permil (‰) relative to the Vienna Pee Dee Belemnite (VPDB) standard.

4. Results

4.1 Base of hydrate stability zone

The bottom water temperature at a water depth of 1033 m in MD161-8 site is 6.6°C. The calculated BGHSZ for the site MD161-8 based on the estimated geothermal gradient of 44°C/km is ~150 mbsf which is close to the observed depth of BSR (~160 mbsf; Collett et al., 2008).

4.2 Grain size distribution

Silt and clay constitute bulk of the sediments (Fig. 2). Silt and clay concentrations in MD161-8 are 24-54 vol% and 45-73 vol% respectively. Relatively high sand concentration (1.8 to 5.5 vol%) is measured within the depth zone of 811 to 1389 cmbsf. In MD161-15, the silt and clay concentrations are 24-58 vol% and 26-74 vol% respectively. Sand is present as a minor components (< 10 vol%) except in few samples within 700-800 mbsf in MD161-15 where maximum sand concentration range from 16 to 31 vol% .

4.3 Foraminifera microstructure

Scanning Electron Microscopic studies (Fig. 3 A-F) of foraminifera tests screened for the C and O isotope analyses show pristine preservation with no evidence of recrystallization or shell dissolution. Pores are open (Fig. 3 B, D) and free of any secondary crystalline fillings. Shells show clear growth layers and knobs. In few specimens intact spines are recorded (Fig. 3C), suggesting excellent preservation of original micro/ultrastructures. Figures 3E and F show smooth surfaces in between the ridges. Lack of infilling in broken shells suggest good preservation of original shell composition.

4.4 Age-depth model

The age-depth model for MD161-8 (Fig. 4) is based on the calibrated radiocarbon ages (Mazumdar et al., 2009) and correlation of our δ¹⁸O profile with the standard δ¹⁸O profile of *G. ruber* from the northern Bay of Bengal (Kudrass *et al.*, 2001). Five marine isotope stages (MIS 5 to 1)

representing glacial and interglacial changes are demarcated in figure 4. The time windows for the Last Glacial maxima (LGM), Bølling-Allerød interstadial (B/A) and Younger Dryas (Y-D) events are demarcated in figure-4. Some of the Dansgaard-Oeschger events (D-O events) correlatable with Kudrass et al. (2001) are plotted in the figure. The age depth model of MD161-15 (Fig. 5) shows markedly high sedimentation rate (53.4 to 319.7 cm/ky) in the upper 9 mbsf. Below the sedimentation rate range from 7.2 to 27.5 cm/ky.

4.5 $\delta^{13}\text{C}$ - $\delta^{18}\text{O}$ values

Negative $\delta^{13}\text{C}$ excursions, P₁ to P₆ (Fig. 6B) and B₁ to B₃ (Fig. 6D) are marked on the $\delta^{13}\text{C}$ profiles of *G. ruber* and *Uvigerina* sp. respectively. P and B stand for planktic and benthic foraminifera respectively (Suppl. Table- 1 and 2). Several minor C isotopic excursions can be seen between P₄-P₆. P₄ to P₆ and B₁ to B₃ show similar relative intensity pattern. Peaks equivalent to P₁ to P₃ are not recorded in the benthic foraminifera profile. The $\delta^{13}\text{C}$ - $\delta^{18}\text{O}$ cross plots for benthic and planktic foraminifera along with authigenic carbonates (Mazumdar et al., 2009) are presented in figure-7A and C. Figure 7B and D represent the cross plots of $\delta^{13}\text{C}$ and $\delta^{18}\text{O}$ data points within the time windows 60208-78508 y (*Uvigerina* sp.) and 59720-78264 y (*G.ruber*) respectively. The C-O isotope profiles within this time window is zoomed in Supplementary figure 2. No significant correlation is observed in either plots.

4.6 Authigenic carbonate and Clam shells.

Tubular and massive carbonate bodies are the dominant authigenic carbonate types recovered from MD161-15 (Fig. 8). Well preserved Scaphopoda shells (benthic burrowing mollusc) are observed cemented on the carbonate structures. Fragments of chemosynthetic clam shells (*Calyplogena* sp. and *Lucinoma* sp.) recovered within the depth range of 27 to 31 mbsf are presented in figure-9. $\delta^{13}\text{C}$ values of four representative carbonate samples are -46.8, -47.3, -47.9 and -50.2 ‰VPDB (Suppl. Table- 3).

4.7 TIC and Organic geochemistry

TIC concentrations range from 0.11 to 2.2 wt% and show marked vertical fluctuation (Fig. 10A). The $\delta^{13}\text{C}_{\text{TIC}}$ data in figure-10A is from Peketi et al. (2012). The total organic carbon contents (Suppl. Table- 4) in MD161-8 varies from 1.1 to 2 wt% (Fig.10B). The TOC/TN ratio in MD161-8 range from 10.4 to 30.6 (avg: 16.1 ±3.5). $\delta^{13}\text{C}_{\text{TOC}}$ profile (Fig. 6E, Suppl. Table-4) shows marked negative

excursion during MIS-4 relative to the average value of -17.0 ± 1.8 ‰ VPDB. The aliphatic hydrocarbon extracts from the sediment samples within this zone show the presence of 2,6,10,15,19-pentamethylcosane (PMI: Fig. 11). PMI could be quantified only in two samples within the depth zone of 16-18 mbsf. Quantification of PMI was done relative to the internal standard. PMI concentration ranges from 0.34 to 0.75 $\mu\text{g/g}$ of dry sediment. $\delta^{13}\text{C}_{\text{PMI}}$ values of two samples reported here are -107 and -139 ‰ VPDB (Fig. 6E).

5. Discussion

5.1 C-O isotopic perturbation: Possible diagenetic influence

Recrystallization of foraminifera shell or precipitation of ^{13}C depleted authigenic carbonate crystals within the shell cavities are the commonly cited causes for highly negative $\delta^{13}\text{C}$ signature of foraminifera shells (Martin et al., 2004; Ohkushi et al., 2005; Wiedicke and Weiss, 2006; Uchida et al., 2008; Torres et al., 2010 and Cook et al., 2011). The shells analysed (Fig. 3) in our study are not brown or yellowish in colour and also do not show any apparent recrystallization features under scanning electron microscope (SEM). In fact, the structures are extremely well preserved (Fig. 3). We also have not observed any authigenic carbonate fillings within the pores or inside the cavities. However, some minute remnants are very difficult to ascertain unless every individual shells analysed for isotopic composition is observed under SEM. In figure-7 A and C no obvious mixing line could be established between the authigenic carbonate and foraminifera data clusters unlike the observation by Wiedicke and Weiss, (2006) from Sunda arc basin. Inclusions of authigenic carbonates with $\delta^{18}\text{O}$ values ranging from +3.2 to +5.2 ‰ VPDB (Fig. 7A and C) would result in ^{18}O enrichment in foraminifera shell and a positive shift in $\delta^{18}\text{O}$ relative to the pristine shells. The effect of contamination with ^{18}O enriched authigenic carbonate is expected to be more prominent in planktonic than benthic foraminifera since benthic forms during MIS-4 are reported to be enriched in ^{18}O (Pitrowski et al., 2009). Figure 7B and D show the data cluster within the time window 60208-78508 y when the most intense ^{13}C depletion is recorded. The data points show no notable correlation. However, the observed similarity of $\delta^{18}\text{O}_{\text{G.ruber}}$ values during MIS-4 and MIS-2 (Fig. 6B) in MD161-8 is contrasting to the observation of Kudrass et al. (2001) from the Bay of Bengal (Fig. 4A). This possibly suggest incorporation of ^{18}O enriched carbonate in the foraminifera at the site (MD161-8). The ^{18}O enrichment may be attributed to the post depositional diagenetic alteration which is not detected by normal visual inspection. The $\delta^{18}\text{O}$ values

possibly resulted by ^{18}O enriched water released during the destabilization of methane hydrate (Matsumoto and Borowski, 2000) or inclusion of undetected ^{18}O enriched authigenic carbonate. Rigorous chemical analyses like Mg/Ca, Mn/Ca ratios and $\Delta^{14}\text{C}$ is required to narrow down the least contaminated shells (Uchida et al., 2008). $^{87}\text{Sr}/^{86}\text{Sr}$ ratio may also help in understanding the sediment porefluid calcite shell interaction. Incorporation of ^{13}C depleted dissolved inorganic carbon (DIC) produced solely via degradation of organic rain cannot explain the repeated spikes in ^{13}C depletion (Stott et al., 2002) in the C- isotope ratio profiles (Fig. 6 B and D) since the TOC content varies within a narrow band (Avg: 1.5 ± 0.2 wt%; Fig. 10B) in MD161-8 and does not show any high concentration spikes correlatable with the planktic or benthic C-isotopic depletions.

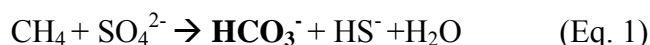
Based on the present observation we cannot rule out the role of diagenetic processes in partially altering the carbon-oxygen stable isotope ratios of the measured foraminifera. However, the lack of visible recrystallization or incorporation of authigenic carbonates fail to provide a comprehensive explanation for the observed episodic isotopic perturbations only through diagenesis, thus leaving the room for at least partial contribution of palaeocenographic processes as one of the possible causative factors as observed by Uchida et al. (2008).

5.2 Methane emission and C isotope perturbation

The negative carbon isotope excursions (Fig. 6B and D) corresponding to P_1 , P_2 and P_3 are not observed in the benthic foraminifera. In other words the processes responsible for changing the carbon isotope ratios of the shallow water bicarbonate reservoir during P_1 , P_2 and P_3 events were apparently decoupled from the deep water bicarbonate pool. Timings of P_2 and P_3 may correspond to the Dansgaard-Oeschger warming events during the 40-50 ky time window (Kudrass et al., 2001). However, it is difficult to relate the observed small carbon isotope perturbation to episodic destabilization of methane hydrate deposits (Kennett et al., 2000; Kennett et al., 2003) of K-G basin in the absence of corresponding ^{13}C depletion in benthic foraminifera and other biological/ geochemical evidence (Mazumdar et al., 2009b). Wetland methane emission could also have influenced the depleted carbon isotopic signature. The negative $\delta^{13}\text{C}$ excursion, P_1 at the LGM, may also be attributed to the upwelling of Southern Ocean deep water with depleted carbon stable isotope ratios (Spero and Lea, 2002) in-to the shallow waters of Northern Indian Ocean during deglaciation. The planktic foraminifera *G.ruber* also show negative carbon isotopic excursions (P_4 , P_5 and P_6) which are stratigraphically close to the

excursion B1, B2 and B3. Compared to the benthic foraminifera, the planktic counterpart shows several excursions close to P4, P5 and P6. A palaeoenvironmental explanation for the ^{13}C depleted planktic foraminifera would involve carbon isotopic alteration of the bicarbonate reservoir of the upper mixed layer (0-25m) by the aerobic oxidation of the methane expelled from the sediment bed (Blumenberg et al., 2007). The volume of methane gas that can reach the shallow waters depends on several factors. Model calculations by Zhang (2003) and Leifer et al. (2006) show that the efficiency of methane ebullition depends on the water depth, magnitude of seepage, upward velocity, bubble size and presence of hydrate coating on methane bubbles (Sauter et al., 2006). However, a direct link between the negative carbon isotopic excursion observed in *G. ruber* and methane flux into the shallow waters is not possible to establish unequivocally in the present work due to the regional nature of the event and possibility of partial diagenetic alterations.

The pulses of depleted carbon isotope excursions in benthic (B_1 , B_2 and B_3) foraminifera possibly suggest that the methane expulsion events during MIS-4 (Glacial stage) and at the transition of MIS-4 and MIS-5 (interglacial), altered the bicarbonate carbon isotopic composition near the sediment water interface (Wefer et al., 1994; Panieri et al., 2012; Wang et al., 2013). A significant fraction of methane is oxidized to HCO_3^- via anaerobic methane oxidation (AMO) close to the sediment water interface. AMO is attributed to a consortium of CH_4 -oxidizing archaea and sulfate-reducing bacteria (Orphan et al., 2001; Reeburgh, 2007; Knittel and Boetius, 2009) and can be represented by equation 1.



Presence of chemosynthetic bivalves like *Calyptogena sp* (Collett et al., 2008; Mazumdar et al., 2009b) and of Mo concentration anomaly within 16-18 mbsf (depth zone of foraminifera carbon isotope anomaly) of core MD161-8 (Peketi et al., 2012), have convincingly demonstrated paleo methane expulsion events and accompanied AMO/ sulfidization at or above the sediment water interface in K-G basin. On the other hand extensive studies on long sediment cores collected from K-G basin, Mazumdar et al. (2012) have shown evidence of recent as well as paleo vertical movement of the sulfate- methane transition zones in the K-G basin due to variations in the methane flux possibly driven by activation of fault system.

Depletion in carbon isotope ratios of the dissolved inorganic carbonate (DIC) pool depends on the carbon stable isotope ratios of methane advecting from the deeper sediment layers. Reported

$\delta^{13}\text{C}_{\text{CH}_4}$ values (-75 to -85 ‰ VPDB) and C1/(C2+C3) ratios (1110 to 3354) by Collett et al., 2008 and Mazumdar et al., 2009b and 2012) suggest the presence of biogenic hydrocarbon gases within the methanogenic zone at the site MD161-8. Carbon isotope values of shallow (top ~ 0.5 cmbsf) infaunal benthic foraminifera such as *Uvigerina* sp. may get significantly influenced by incorporation of bicarbonate with isotopically depleted carbon in the calcitic shell during growth (Hill et al., 2003 and 2004b). Carbon isotopic composition of benthic foraminifera may also be influenced by the carbon isotope ratios of food source (Panieri et al., 2009). The presence of 2,6,10,15,19-pentamethylcosane (PMI) an archaeal membrane lipid biomarker with extremely depleted carbon isotope ratios (-106 to -139 ‰ VPDB) suggest AOM and enhanced abundances of methanotrophic archaeal biomass governed by methane emission (Orphan et al., 2001; Thiel et al., 2001; Peckmann and Thiel, 2004; Zhiguang and Wang, 2006). Niemann et al. (2006) reported PMI from methane seepage related carbonate crust from gulf of Cadiz mud volcano. The free energy yield (-25 kJ mol⁻¹), ANME cell count (<10⁶ cells cm⁻³) and AOM rate (< 10 nmol cm⁻³ day⁻¹) reported from the deep SMTZ below seafloor are lower, compared to those from seep/ vent sites (Valentine and Reeburgh, 2000; Valentine, 2002; Knab et al., 2008; Harrison et al., 2009; Knittel and Boetius, 2009). The sharp negative excursion in the bulk $\delta^{13}\text{C}_{\text{TOC}}$ (Fig. 6E) within 16-18 mbsf possibly reflect the incorporation of isotopically depleted archaeal biomass in the sediment. Lack of correlatable change in TOC/TN ratio with the $\delta^{13}\text{C}_{\text{TOC}}$ spikes rules out high marine productivity as a reason for the ¹²C enriched TOC. Benthic foraminifera feeding on such microbial mats may grow tests with markedly depleted carbon isotope ratios (Sen Gupta et al., 1997; Levin and Michener, 2002). Depleted carbon isotope ratios in benthic foraminifera are considered as a potential proxy for paleo-methane seepage (Wefer et al., 1994; Kennett et al., 1996; Sen Gupta et al., 1997; Rathburn et al., 2000). However, the interpretation of seepage indicator need more detailed investigation since PMI has also been reported from SMTZ deeper within the sediment (Lee et al., 2013, Weijers et al., 2011; Aquilina et al., 2010).

5.3 Gas hydrate destabilization: Tectonics and perturbed P-T condition

Thermodynamic calculations based on hydrate stability equations (Sloan, 1998) show that the present base of the gas hydrate stability zone (BGHSZ) in offshore K-G basin is ~150 mbsf which is close the depth of BSR (~160 mbsf). Bright spots, acoustic blanking/turbidity and drop in P-wave velocity below BSR testify the presence of free gas (Dewangan et al., 2010; Shankar and Riedel, 2010). Based on the enrichment in the oxygen isotope and Mg/Ca ratios in benthic foraminifera (Martin et al.,

2002; Waelbroeck et al., 2002), temperature drop (relative to present) of ~2 and 3 °C can be estimated for the deep waters of the equatorial/tropical Pacific and southern Indian oceans respectively during MIS-4. Since no bottom water temperature estimation is available for the late Quaternary from northern Indian Ocean, we assume that the bottom water temperature during MIS 4 was at least 1-2 degree lower than that of the present (6.6 °C) at our sampling depth. Based on SPECMAP data, the estimated sea level was ~90 to 95 m below present during the MIS-4 and at the transition of MIS-5 to MIS-4 (Berné et al., 2004). Calculations using different combination of P-T conditions show that BGHSZ was possibly deeper by ~10 to 36 m relative to the present depth of BGHSZ (~150 mbsf) thus increasing the methane hydrate stability zone. Moreover, the record of benthic foraminifera $\delta^{18}\text{O}$ pattern (Fig. 6C) does not support rapid or episodic bottom water warming corresponding to the depleted carbon isotopic excursions (Fig. 6D). However, assuming no reduction in bottom water temperature relative to the present, a S.L. drop of 90-95 m would destabilize the methane hydrate and push the BGSHZ upward by ~16 m. This would result in the generation of free gas which may emit out of the sea bed if conduits are available. However, in either case, conduits in the form of fault systems requires passive tectonics processes typically associated with shale tectonism in K-G basin. Sustaining flow of methane gas through conduits across the hydrate stability zone has to be facilitated by additional physicochemical conditions like warm fluid or enhanced salinity to avoid hydrate crystalization.

Shale tectonics (diapirism) induced deep fault system has been amply demonstrated from the K-G Basin (Mazumdar et al., 2009b; Dewangan et al., 2010; Shankar and Riedel, 2010; Riedel et al., 2010; Choudhury et al., 2011). Shale tectonic is driven by the downward movement of thick sediment mass over a deeply buried over pressured shale strata (Damuth, 1994; Wu and Bally, 2000). The perturbation of the over pressured strata induces folding, faulting and upthrusting of the overburden strata thereby creating prominent bathymetric mounds and ridges (Rao and Mani, 1993; Dewangan et al., 2010). Migration through the deep fault systems possibly played an important role in advection of the fluids (Shankar and Riedel, 2010; Dewangan et al., 2011; Jaiswal et al., 2012). Fluids advecting from greater depths are likely to be much warmer than the shallow sediments in the GHSZ (Max et al., 2006). The increase in geothermal gradient (calculated using BSR) in the vicinity of the studied core (Dewangan et al., 2011) suggest advection of warm fluid through the contemporaneous fault systems resulting in focused fluid flow (Carson and Sreaton, 1998). The episodic nature of the carbon isotopic excursions (Fig. 6B and D) suggests periodic quiescence or reactivation of fault system. This association in K-G basin is further supported by the record of paleo- methane seepage related authigenic carbonate deposits

at the site MD161-15. The wet bulk density (Dewangan et al., 2010) of the core MD161-15 also shows the occurrences of lithified authigenic carbonates within a depth zone of 27 to 31 mbsf (Fig. 5D). The tubular shaped carbonate structures (Fig. 10) with strong depletion in carbon isotope ratios (Table TS 5) and presence of fossil shells of shallow surface dwelling or burrowing mollusk (Scaphopoda) suggest near surface precipitation of high magnesian carbonates at MD161-15 due to methane emission and anaerobic oxidation of methane (Suppl. Table -3). Methane expulsion is further supported by the record of chemosynthetic clam shells (*Calyptogena and Lucinoma* sp.) from the authigenic carbonate rich horizons (Fig. 11). Earlier Mazumdar et al. (2009) reported these type of clam shells from core MD161-8. The timing of this methane seepage event recorded in MD 161-15 is yet to be determined. Like MD161-8, the coring site MD161-15 is also located on a shale tectonics induced mound overlying a gas hydrate deposit. Evidence from of methane emission events from the two sites located on mounds in K-G basin supports the link between passive tectonics induced fault/ and methane emission events in K-G basin.

6. Conclusions

We have recorded negative spikes (P₄-P₆ and B₁-B₃) of carbon isotope ratios in the planktic (*G. ruber*) and benthic (*Uvigerina* sp.) foraminifera within MIS-4 and at the transition of MIS-5 and 4 which can be correlated with methane expulsion events in K-G basin, Bay of Bengal. The influence of diagenetic modification on the isotopic signals can not be ruled out in the present study. The negative excursions observed in benthic foraminifera are significantly larger than in the planktic counterpart. The carbon isotopic perturbations in the foraminifera in MD161-8 can be correlated with the earlier reports on occurrence of chemosynthetic bivalve fossils and positive Mo anomaly within same time window. The above observations have attributed to methane emission event likely caused by methane hydrate destabilization. The hydrate destabilization and methane emission event in K-G basin has been linked to shale tectonic events leading to fracture and fault generation which provided the vertical conduit for the emission of methane gas. We suggest that the globally recorded shale and salt tectonics and associated focused fluid flow in passive continental margins play an important role in marine methane seepage events.

Acknowledgements

We thank the directors of CSIR-NIO, NIOT, NCAOR and advisor MOES for supporting this study. Head, oceanography department, and in-charge on-board operations of IPEV are thanked for providing onboard technical support and facilities. Funding support to RJ and AP from CSIR and VNJCT are sincerely acknowledged. Mr. G. Prabhu and Mr. V.D. Khedekar/A. Sardar helped in acquiring XRD and SEM data at NIO respectively.

References:

- Aquilina, A., Knab, N. J., Knittel, K., Kaur, G., Geissler, A., Kelly, S. P., Fossing, H., [Boot](#), C. S., [Parkes](#), R. J., [Mills](#), R. A., [Boetius](#), A., [Lloyd](#), J. R., Pancost, R. D., 2010. Biomarker indicators for anaerobic oxidizers of methane in brackish-marine sediments with diffusive methane fluxes. *Organic Geochemistry*, 41, 414-426.
- Archer, D., 2007. Methane hydrate stability and anthropogenic climate change. *Biogeosciences Discussions* 4, 993-1057.
- Berné, S., Rabineau, M., Flores, J.A., Sierro, F.J., 2004. The impact of Quaternary global changes on strata formation: exploration of the shelf edge in the Northwest Mediterranean Sea. *Oceanography* 17, 92-103.
- Blumenberg, M., Seifert, R., Michaelis, W., 2007. Aerobic methanotrophy in the oxic-anoxic transition zone of the Black Sea water column. *Org. Geochem.* 38, 84-91.
- Bock, M., Schmitt, J., Möller, L., Spahni, R., Blunier, T., Fischer, H., 2010. Hydrogen isotopes preclude marine hydrate CH₄ emissions at the onset of Dansgaard-Oeschger events. *Science* 328, 1686-1689.
- Buffett, B., Archer, D., 2004. Global inventory of methane clathrate: sensitivity to changes in the deep ocean. *Earth Planet. Sci. Lett.* 227, 185-199.
- Carson, B., Sreaton, E.J., 1998. Fluid flow in accretionary prisms: Evidence for focused, time-variable discharge. *Rev. of Geophys.* 36, 329-351.
- Chanton, J.P., Whiting, G.J., 1996. Methane stable isotopic distributions as indicators of gas transport mechanisms in emergent aquatic plants. *Aqu. Botany* 54, 227-236.
- Chappellaz, J., Blunier, T., Kints, S., Dallenbach, A., Barnola, J.M., Schwander, J., Raynaud, D., Stauffer, B., 1997. Changes in the atmospheric CH₄ gradient between Greenland and Antarctica during the Holocene. *J. Geophys. Res. Atmosph.* 102, 15987-15997.
- Choudhori, M., Guha, D., Dutta, A., Sinha, S., and Sinha, N., 2011. Spatiotemporal Variations and Kinematics of Shale Mobility in the Krishna-Godavari Basin, India. In AAPG Memoir 93 Shale

Tectonics, Ed. Wood, L.H., pp. 91-110.

Coffin, R. B., Smith, J. P., Plummer, R. E., Yoza, B., Larsen, R. K., Millholland, L. C., Montgomery, M. T., 2013. Spatial variation in shallow sediment methane source and cycling on the Alaskan Beaufort Sea shelf/ slope. *Mar. Pet. Geol.* 45, 186-197.

Collett, T., Riedel, M., Cochran, J., Boswell, R., Presley, J., Kumar, P., Sathe, A., Sethi, A., Lall, M., Sibal, V., 2008. National Gas Hydrate Program: Expedition 01, Initial Reports, vol. 1, Dir. Gen. of Hydrocarbon, New Delhi, India.

Cook, M.S., Keigwin, L.D., Birgel, D., Hinrichs, K.-U., 2011. Repeated pulses of vertical methane flux recorded in glacial sediments from the southeast Bering Sea. *Paleoceanography* 26, 1-17.

Dällenbach, A., Blunier, T., Fluckiger, J., Stauffer, B., Chappellaz, J., Raynaud, D., 2000. Changes in the atmospheric CH₄ gradient between Greenland and Antarctica during the Last Glacial and the transition to the Holocene. *Geophys. Res. Lett.* 27, 1005-1008.

Damuth, J.E., 1994. Neogene gravity tectonics and depositional processes on the deep Niger Delta continental margin. *Mar. Pet. Geol.* 11, 320-346.

De Garidel-Thoron, T., Beaufort, L., Bassinot, F., Henry, P., 2004. Evidence for large methane releases to the atmosphere from deep-sea gas-hydrate dissociation during the last glacial episode. *Proceedings of the National Academy of Sciences of the United States of America* 101, 9187-9192.

Dewangan, P., Ramprasad, T., Ramana, M., Mazumdar, A., Desa, M., Badesab, F.K., 2010. Seabed Morphology and Gas Venting Features in the Continental Slope Region of Krishna-Godavari Basin, Bay of Bengal: Implications in Gas-Hydrate Exploration. *Mar. Pet. Geol.* 27, 1628-1641.

Dewangan, P., Sriram, G., Ramprasad, T., Ramana, M., Jaiswal, P., 2011. Fault system and thermal regime in the vicinity of site NGHP-01-10, Krishna-Godavari basin, Bay of Bengal, *Mar. Pet. Geol.* 28, 1899-1914.

Dickens, G.R., 2003. Rethinking the global carbon cycle with a large, dynamic and microbially mediated gas hydrate capacitor. *Earth Planet. Sci. Lett.* 213, 169-183.

Dickens, G., O'Neil, J., Rea, D., Owen, R., 1995. Dissociation of oceanic methane hydrate as a cause of the carbon isotope excursion at the end of the Paleocene. *Paleoceanography* 10, 965-971.

Etioppe, G., Lassey, K.R., Klusman, R.W., Boschi, E., 2008. Reappraisal of the fossil methane budget and related emission from geologic sources. *Geophys. Res. Lett.* 35, L09307.

Hardy, R., Tucker, M., 1988. X-ray powder diffraction of sediments. *Techniques in Sedimentology*, edited by, M. Tucker, pp 191-228, Blackwell Scientific Publication, Oxford, U.K.

Harrison, B.K., Zhang, H., Berelson, W., Orphan, V.J., 2009. Variations in archaeal and bacterial diversity associated with the sulfate-methane transition zone in continental margin sediments (Santa Barbara Basin, California). *Applied and Environmental Microbiology* 75, 1487-1499.

Herguera, J. C., C. K. Paull, E. Perez, W. Ussler III, and E. Peltzer, 2014, Limits to the sensitivity of living benthic foraminifera to pore water carbon isotope anomalies in methane vent environments, *Paleoceanography* 29, 273–289.

Hill, T.M., Kennett, J.P., Spero, H.J., 2003. Foraminifera as indicators of methane-rich environments: A study of modern methane seeps in Santa Barbara Channel, California. *Mar. Micropal.* 49, 123-138.

Hill, T.M., Kennett, J.P., Spero, H.J., 2004a. High-resolution records of methane hydrate dissociation: ODP Site 893, Santa Barbara Basin. *Earth Planet. Sci.* 223, 127-140.

Hill, T.M., Kennett, J.P., Valentine, D.L., 2004b. Isotopic evidence for the incorporation of methane-derived carbon into foraminifera from modern methane seeps, Hydrate Ridge, Northeast Pacific. *Geochim. Cosmochim. Acta* 68, 4619-4627.

Hinrichs, K.U., Hmelo, L.R., Sylva, S.P., 2003. Molecular fossil record of elevated methane levels in late Pleistocene coastal waters. *Science* 299, 1214-1217.

Hovland, M., Judd, A.G., 1992. The global production of methane from shallow submarine sources. *Continental Shelf Res.* 12, 1231-1238.

Jahren, A.H., Arens, N.C., Sarmiento, G., Guerrero, J., Amundson, R., 2001. Terrestrial record of methane hydrate dissociation in the Early Cretaceous. *Geology* 29, 159-162.

Jaiswal, P., Dewangan, P., Ramprasad, T., Zelt, C.A., 2012. Seismic characterization of hydrates in faulted, fine-grained sediments of Krishna-Godavari basin: Unified imaging. *J. Geophys. Res.* 117, B10305.

Judd, A.G., Hovland, M., Dimitrov, L.I., Garcia Gil, S., Jukes, V., 2002. The geological methane budget at continental margins and its influence on climate change. *Geofluids* 2, 109-126.

Kaplan, J.O., 2002. Wetlands at the Last Glacial Maximum: Distribution and methane emissions. *Geophys. Res. Lett.* 29.

Kemp, D.B., Coe, A.L., Cohen, A.S., Schwark, L., 2005. Astronomical pacing of methane release in the Early Jurassic period. *Nature* 437, 396-399.

Kennedy, M., Mrofka, D., von der Borch, C., 2008. Snowball Earth termination by destabilization of equatorial permafrost methane clathrate. *Nature* 453, 642-645.

Kennett, J., Cannariato, K., Hendy, I., Behl, R., 2000. Carbon isotopic evidence for methane hydrate instability during Quaternary interstadials. *Science* 288, 128-133.

Kennett, J. P., Cannariato, K. G., Hendy, I. L., Behl, R. J., 2003. Methane hydrates in Quaternary climate change: The clathrate gun hypothesis. *Amer Geophysical Union*, 216 pp., Washington, DC.

Kennett, J.P., Stott, L.D., 1991. Abrupt deep sea warming, paleoceanographic changes and benthic extinctions at the end of the Paleocene. *Nature* 353, 225-229.

Kennett, J. P., Hendy, I. L., Behl, R. J., 1996. Late Quaternary foraminiferal carbon isotopic record in Santa Barbara Basin: Implications for rapid climate change, *EOS Trans.*, AGU 77 (46), 294.

Knab, N.J., Cragg, B.A., Borowski, C., Parkes, R.J., Pancost, R., Jørgensen, B.B., 2008. Anaerobic oxidation of methane (AOM) in marine sediments from the Skagerrak (Denmark): I. Geochemical and microbiological analyses. *Geochim. Cosmochim. Acta* 72, 2868-2879.

Knittel, K., Boetius, A., 2009. Anaerobic oxidation of methane: progress with an unknown process. *Annual review of microbiology* 63, 311-334.

Kudrass, H., Hofmann, A., Dose, H., Emeis, K., Erlenkeuser, H., 2001. Modulation and amplification of climatic changes in the Northern Hemisphere by the Indian summer monsoon during the past 80 ky. *Geology* 29, 63-66.

Kvenvolden, K.A., Lorenson, T.D., 2001. The global occurrence of natural gas hydrate. in *Natural Gas Hydrate: Occurrence, Distribution and Detection*, *Geophys. Monogr. Ser.*, vol. 124, edited by C.K Paul and W.P Dillon, pp. 3-18. AGU, Washinton, D.C.

Kvenvolden, K., 1993. Gas hydrates—geological perspective and global change. *Rev. Geophys* 31, 173–187.

Lashof, D.A., Ahuja, D.R., 1990. Relative contributions of greenhouse gas emissions to global warming. *Nature* 344, 529-531.

Lee, D. H., Kim, J. H., Bahk, J. J., Cho, H. Y., Hyun, J. H., Shin, K. H., 2013. Geochemical signature related to lipid biomarkers of ANMEs in gas hydrate-bearing sediments in the Ulleung Basin, East Sea (Korea). *Marine and Petroleum Geology* 47, 125-135.

Leifer, I., Luyendyk, B.P., Boles, J., Clark, J.F., 2006. Natural marine seepage blowout: Contribution to atmospheric methane. *Global biogeochemical cycles* 20, GB3008.

Levin, L.A., Michener, R.H., 2002. Isotopic evidence for chemosynthesis-based nutrition of macrobenthos: the lightness of being at Pacific methane seeps. *Limnol. Oceanogr.* 47, 1336-1345.

Martin, P.A., Lea, D.W., Rosenthal, Y., Shackleton, N.J., Sarnthein, M., Papenfuss, T., 2002. Quaternary deep sea temperature histories derived from benthic foraminiferal Mg/Ca. *Earth Planet. Sci. Lett.* 198, 193-209.

Martin, J.B., Day, S.A., Rathburn, A.E., Perez, M.E., Mahn, C., Gieskes, J., 2004. Relationships between the stable isotopic signatures of living and fossil foraminifera in Monterey Bay, California. *Geochem. Geophys. Geosyst.* 5, Q04004.

Matsumoto, R., Borowski, W. S., 2000. Gas hydrate estimates from newly determined oxygen isotopic fractionation (α GH-IW) and $\delta^{18}\text{O}$ anomalies of the interstitial waters: Leg 164, Blake Ridge, *Proc. Ocean Drill. Program Sci. Results* 164, 59–66.

Max, M.D., Johnson, A.H., Dillon, W.P., 2006. *Economic geology of natural gas hydrate*. Dordrecht, Netherlands, 341pp. Springer publishers.

Mazumdar, A., Peketi, A., Dewangan, P., Badesab, F., Ramprasad, T., Ramana, M.V., Patil, D., J., Dayal, A., 2009a. Shallow gas charged sediments off the Indian west coast: Genesis and distribution. *Mar. Geol.* 267, 71-85.

Mazumdar, A., Dewangan, P., João, H.M., Peketi, A., Khosla, V., Kocherla, M., Badesab, F.K., Joshi, R.K., Roxanne, P., Ramamurty, P.B., Karisiddaiah, S. M., Patil, D. J., Dayal, A. M., Ramprasad, T., Hawkesworth, C. J., Avanzinelli, R., 2009b. Evidence of paleo-cold seep activity from the Bay of Bengal, offshore India. *Geochem. Geophys. Geosyst.* 10, Q06005.

Mazumdar, A., Joshi, R.K., Peketi, A., Kocherla, M., 2011. Occurrence of faecal pellet-filled simple and composite burrows in cold seep carbonates: A glimpse of a complex benthic ecosystem. *Mar. Geol.* 289, 117-121.

Mazumdar, A., H.M. Joao, A. Peketi, P. Dewangan, M. Kocherla, R.K. Joshi, Ramprasad, T., 2012. Geochemical and geological constraints on the composition of marine sediment pore fluid: Possible link to gas hydrate deposits. *Mar. Pet. Geol.* 38, 35-52.

Niemann, H., Duarte, J., Hensen, C., Omoregie, E., Magalhaes, V. H., Elvert, M., Pinheiro, L. M. Kopf, A. Boetius, A., 2006. Microbial methane turnover at mud volcanoes of the Gulf of Cadiz. *Geochim. Cosmochim. Acta* 70, 5336-5355.

Ohkushi, K.i., Ahagon, N., Uchida, M., Shibata, Y., 2005. Foraminiferal isotope anomalies from northwestern Pacific marginal sediments. *Geochem. Geophys. Geosyst.* 6, Q04005.

Orphan, V.J., House, C.H., Hinrichs, K.U., McKeegan, K.D., DeLong, E.F., 2001. Methane-consuming archaea revealed by directly coupled isotopic and phylogenetic analysis. *Science* 293, 484-487.

Panieri, G., Camerlenghi, A., Conti, S., Pini, G.A., Cacho, I., 2009. Methane seepages recorded in benthic foraminifera from Miocene seep carbonates, Northern Apennines (Italy). *Palaeo. Palaeo.* 284, 271-282.

Panieri, G., Camerlenghi, A., Cacho, I., Cervera, C.S., Canals, M., Lafuerza, S., Herrera, G., 2012. Tracing seafloor methane emissions with benthic foraminifera: Results from the Ana submarine landslide (Eivissa Channel, Western Mediterranean Sea). *Mar. geol.* 291, 97-112.

Peckmann, J., Thiel, V., 2004. Carbon cycling at ancient methane-seeps. *Chem. Geol.* 205, 443-467.

Peketi, A., Mazumdar, A., Joshi, R.K., Patil, D., Srinivas, P., Dayal, A., 2012. Tracing the Paleo sulfate-methane transition zones and H₂S seepage events in marine sediments: An application of C-S-Mo systematics. *Geochem. Geophys. Geosyst.* 13, Q10007.

Petrenko, V. V., Smith, A. M., Brook, E. J., Lowe, D., Riedel, K., Brailsford, G., & Severinghaus, J. P., 2009. ¹⁴CH₄ measurements in Greenland ice: investigating last glacial termination CH₄ sources. *Science* 324, 506-508.

Pitrowski, A.M., Banakar, V.K., Scrivner, A.E., Elderfield, H., Galy, A., Dennis, A., 2009. Indian Ocean circulation and productivity during the last glacial cycle. *Earth Planet. Sci. Lett.* 285, 179-189.

Ramana, M., Ramprasad, T., Raju, K., Desa, M., 2007. Occurrence of gas hydrates along the continental margins of India, particularly the Krishna-Godavari offshore basin. *Intern. J. Environ. Studies.* 64, 675-693.

Rao, G., 2001. Sedimentation, stratigraphy, and petroleum potential of Krishna-Godavari basin, East Coast of India. *Amer. Assoc. Petrol. Geol.* 85, 1623-1643.

Rao, G., Mani, K., 1993. A study on generation of abnormal pressures in Krishna Godavari basin. *Indian J. Petrol. Geol.* 2, 20-30.

Rathburn, A.E., Levin, L.A., Held, Z., Lohmann, K.C., 2000. Benthic foraminifera associated with cold methane seeps on the northern California margin: ecology and stable isotopic composition. *Marine Micropal.* 38, 247-266.

Reeburgh, W.S., 2007. Oceanic methane biogeochemistry. *Chem. Rev.* 107, 486-513.

Riedel, M., Collett, T., Kumar, P., Sathe, A., Cook, A., 2010. Seismic imaging of a fractured gas hydrate system in the Krishna-Godavari Basin offshore India. *Mar. Pet. Geol.* 27, 1476-1493.

Sanchez Goni, M.F., Landais, A., Fletcher, W.J., Naughton, F., Desprat, S., Duprat, J., 2008. Contrasting impacts of Dansgaard-Oeschger events over a western European latitudinal transect modulated by orbital parameters. *Quat. Sc. Rev.* 27, 1136-1151.

Sauter, E.J., Muyakshin, S.I., Charlou, J.L., Schluter, M., Boetius, A., Jerosch, K., Damm, E., Foucher, J.-P., Klages, M., 2006. Methane discharge from a deep-sea submarine mud volcano into the upper water column by gas hydrate-coated methane bubbles. *Earth Planet. Sci. Lett.* 243, 354-365.

Sen Gupta, B.K., Platon, E., Bernhard, J.M., Aharon, P., 1997. Foraminiferal colonization of hydrocarbon-seep bacterial mats and underlying sediment, Gulf of Mexico slope. *J. Foraminiferal Res.* 27, 292-300.

Shankar, U., Riedel, M., 2010. Seismic and heat flow constraints from the gas hydrate system in the Krishna-Godavari Basin, India. *Mar. Geol.* 276, 1-13.

Singh, S.C., Minshull, T.A., Spence, G.D., 1993. Velocity structure of a gas hydrate reflector. *Science* 260, 204-207.

Sloan, E. D., 1998. *Clathrate hydrates of natural gases.* (2nd edition), 730 pp., New York, Marcel Dekker Inc.

Smith, L. M., Sachs, J. P., Jennings, A. E., Anderson, D. M., deVernal, A., 2001. Light $\delta^{13}\text{C}$ events during deglaciation of the East Greenland continental shelf attributed to methane release from gas hydrates. *Geophys. Res. Lett.* 28, 2217-2220.

Spero, H.J., Lea, D.W., 2002. The cause of carbon isotope minimum events on glacial terminations. *Science* 296, 522-525.

Sowers, T., 2006. Late quaternary atmospheric CH₄ isotope record suggests marine clathrates are stable. *Science* 311, 838-840.

Stott, L.D., Bunn, T., Prokopenko, M., Mahn, C., Gieskes, J., Bernhard, J.M., 2002. Does the oxidation of methane leave an isotopic fingerprint in the geologic record? *Geochem. Geophys. Geosyst.* 3.

Thiel, V., Peckmann, J., Richnow, H. H., Luth, U., Reitner, J., Michaelis W., 2001. Molecular signals for anaerobic methane oxidation in Black Sea seep carbonates and a microbial mat, *Mar. Chem.* 73, 97–112.

Torres, M.E., Martin, R.A., Klinkhammer, G.P., Nesbitt, E.A., 2010. Post depositional alteration of foraminiferal shells in cold seep settings: new insights from flow-through time-resolved analyses of biogenic and inorganic seep carbonates. *Earth Planet. Sci. Lett.* 299, 10-22.

Uchida, M., Shibata, Y., Ohkushi, K.i., Ahagon, N., Hoshiya, M., 2004. Episodic methane release events from Last Glacial marginal sediments in the western North Pacific. *Geochem. Geophys. Geosyst.* 5, Q08005.

Uchida, M., Ohkushi, K.i., Kimoto, K., Inagaki, F., Ishimura, T., Tsunogai, U., TuZino, T., Shibata, Y., 2008. Radiocarbon-based carbon source quantification of anomalous isotopic foraminifera in last glacial sediments in the western North Pacific. *Geochem. Geophys. Geosyst.* 9.

Valentine, D.L., 2002. Biogeochemistry and microbial ecology of methane oxidation in anoxic environments: a review. *Antonie Van Leeuwenhoek* 81, 271-282.

Valentine, D., Reeburgh, W., 2000. New perspectives on anaerobic methane oxidation. *Environ. Microbiol.* 2, 477-484.

Waelbroeck, C., Labeyrie, L., Michel, E., Duplessy, J.C., McManus, J.F., Lambeck, K., Balbon, E., Labracherie, M., 2002. Sea-level and deep water temperature changes derived from benthic foraminifera isotopic records. *Quat. Sci. Rev.* 21, 295-305.

Walter, K.M., Zimov, S.A., Chanton, J.P., Verbyla, D., Chapin, F.S., 2006. Methane bubbling from Siberian thaw lakes as a positive feedback to climate warming. *Nature* 443, 71-75.

Wang, S., Yan, B., Yan, W., 2013. Tracing seafloor methane emissions with benthic foraminifera in the Baiyun Sag of the northern South China Sea. *Environ. Earth Sci.* 70, 1143-1150.

Wefer, G., Heinze, P.M., Berger, W.H., 1994. Clues to ancient methane release. *Nature* 369, 282.

Weijers, J. W., Lim, K. L., Aquilina, A., Sinninghe Damsté, J. S., & Pancost, R. D., 2011. Biogeochemical controls on glycerol dialkyl glycerol tetraether lipid distributions in sediments characterized by diffusive methane flux. *Geochemistry, Geophysics, Geosystems*, 12, 1-15

Wiedicke, M., Weiss, W., 2006. Stable carbon isotope records of carbonates tracing fossil seep activity off Indonesia. *Geochem. Geophys. Geosyst.* 7.

Wolff, E., Spahni, R., 2007. Methane and nitrous oxide in the ice core record. *Philosophical Transactions of the Royal Society A: Mathematical, Physical and Engineering Sciences* 365, 1775-1792.

Wu, S., Bally, A.W., 2000. Slope Tectonics-comparisons and Contrasts of Structural Styles of Salt and Shale Tectonics of the Northern Gulf of Mexico with Shale Tectonics of Offshore Nigeria in Gulf of Guinea. *Atlantic rifts and continental margins* 115, 151-172.

Zhang, Y., 2003. Methane escape from gas hydrate systems in marine environment, and methane-driven oceanic eruptions, *Geophys. Res. Lett.* 30, 51-1 to 51-4, doi:10.1029/2002GL016658.

Zhiguang, S., Wang, C., 2006. The biomarkers of 2,6,10,15, 19-pentamethylcosenes and their carbon isotopic composition in the sediments from the Gulf of Mexico. *Chinese Sci.Bull.* 51, 1736-1740.

Figure and Table Captions

Figure-1. Contour map of K-G Basin showing core locations of MD161-8 and 15 and NGHP10-D, 5D and 6C.

Figure 2. Grain size and wet bulk density data of MD161-8 and MD161-15. The rectangular box in B and D represents zone of authigenic carbonate enrichment. Chemosynthetic clam shell occurrences and Mo concentration anomaly are reported with the depth zone of 16-18 mbsf (box in B)

Figure-3 Scanning electron micrographs of representative samples of *G. ruber* and *Uvigerina* sp. analysed for carbon and oxygen stable isotope ratio in core MD161-8. (A, C) *G. ruber* with clean outer shell surface and open pores. (B, D). Arrow in C shows well preserved spines. (E, F) *Uvigerina* sp. showing smooth outer shell surface and well preserved ornamentations.

Figure-4. An age model for the core MD161-8. A. $\delta^{18}\text{O}_{G.ruber}$ profile from Bay of Bengal (modified after Kudrass *et al.* 2001), B. $\delta^{18}\text{O}_{G.ruber}$ profile of MD161-8 from K-G basin, Bay of Bengal. YD= younger Dryas, B/Å = Bølling-Allerød interstadial, LGM = last glacial maxima. D-O = Dansgaard-Oeschger events.

Figure-5. An age model for the core MD161-15.

Figure 6. (A-D) $\delta^{18}\text{O}$ and $\delta^{13}\text{C}$ profiles for *G.ruber* and *Uvigerina* sp in core MD161-8. P₁ to P₆ and B₁ to B₃ represent $\delta^{13}\text{C}$ peaks of planktic and benthic foraminifera respectively. YD, B/Å, D-O, MIS and LGM represent the Younger Dryas, Bølling/Ållerød, Dansgaard-Oeschger, marine isotope stages and last glacial maxima respectively. The colored zone represents different marine isotope stages. (E) Bulk organic matter carbon stable isotope ratios and TOC/TN ratios of MD161-8. Samples enriched in PMI are marked by arrows. The carbon isotope ratios are given in bracket as permil VPDB.

Figure 7. Cross plot of $\delta^{13}\text{C}$ and $\delta^{18}\text{O}$ of benthic (A and B) and planktic (C and D) foraminifera in MD161-8, along with authigenic carbonate data from MD161-8 from Mazumdar *et al.*,2009.

Figure 8. A. Morphology of authigenic carbonates and shells in the carbonate riched zone of MD161-15. (i-iv) Mudstone concretion with gas flow conduit (chimney). (v-vi) Scaphopoda shell penetrating into the carbonate sediment.

Figure 9. A and B. Fragment of *Calypptogena* sp. shell external and internal surfaces, C. external surface of *Lucinoma* sp. The shell fragments are recovered from MD161-15. The gray colored sediment adhered to the shell surfaces are the authigenic carbonates.

Figure 10A. Total inorganic carbon content (TIC wt%) and $\delta^{13}\text{C}_{\text{TIC}}$ profile of MD161-8. $\delta^{13}\text{C}_{\text{TIC}}$ values are from Peketi *et al.* (2012); 10B. TOC content (TOC wt%) of MD161-8.

Figure 11. GC-MS spectra showing PMI peak (short arrow) and structure of 2,6,10,15,19-pentamethylcosane. PMI data is from MD161-8.

Supplementary Table and Figure captions

Suppl. Table 1. Carbon and oxygen stable isotope ratios of planktic foraminifera (*G. ruber*) of MD161-8.

Suppl. Table- 2. Carbon and oxygen stable isotope ratios of benthic foraminifera (*Uvigerina sp*) of MD161-8.

Suppl. Table-3. Mineralogy and $\delta^{13}\text{C}$ - $\delta^{18}\text{O}$ values of authigenic carbonate samples from MD161-15.

Suppl. Table-4. Total organic carbon content (TOC wt %), $\delta^{13}\text{C}_{\text{TOC}}$ (‰ VPDB) and Total inorganic carbon content (TIC wt%) in MD161-8.

Supplementary Figure

Suppl. Figure-1. Temperature, salinity and dissolved oxygen profiles of sea water column near site MD161-8.

Suppl. Figure-2. Blowup of the benthic and planktic foraminifera carbon and oxygen isotope profiles within the age bracket (59000-79000 y BP).

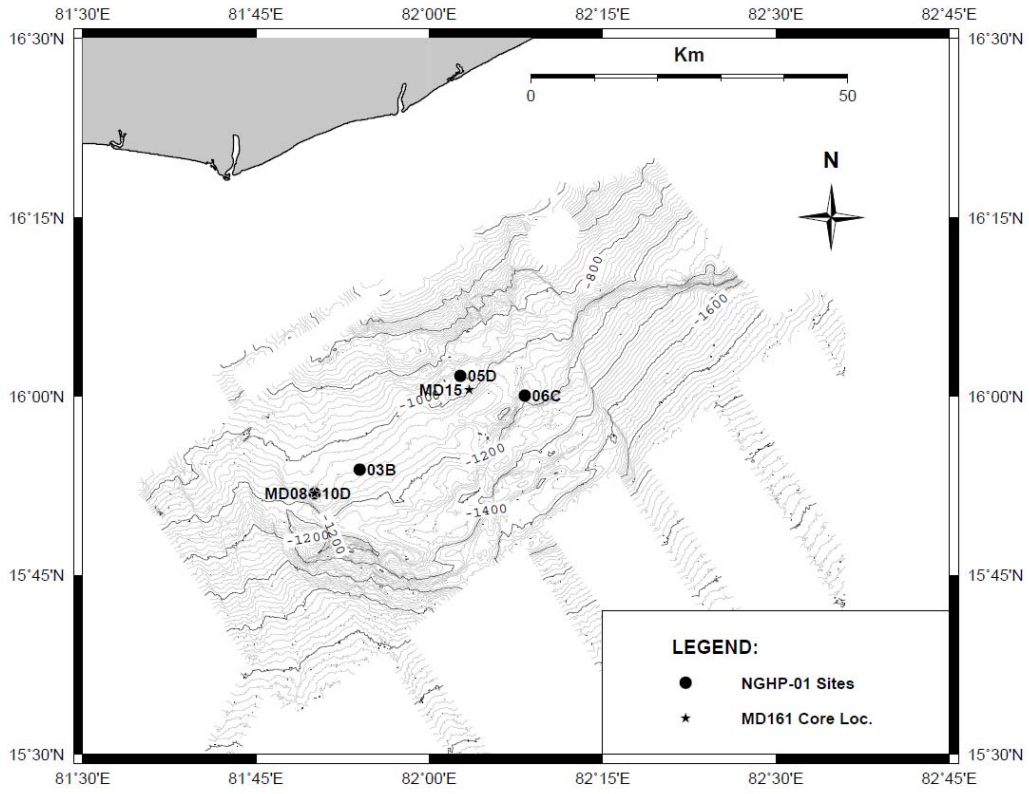


Fig.1

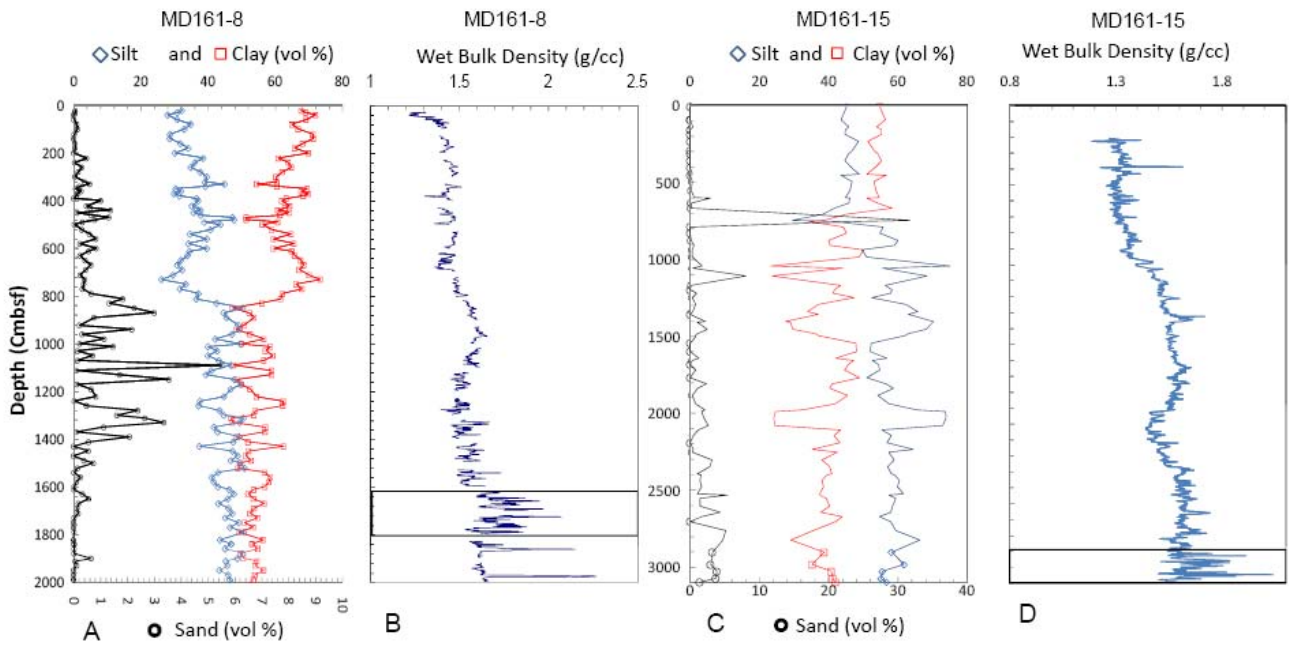


Fig.2

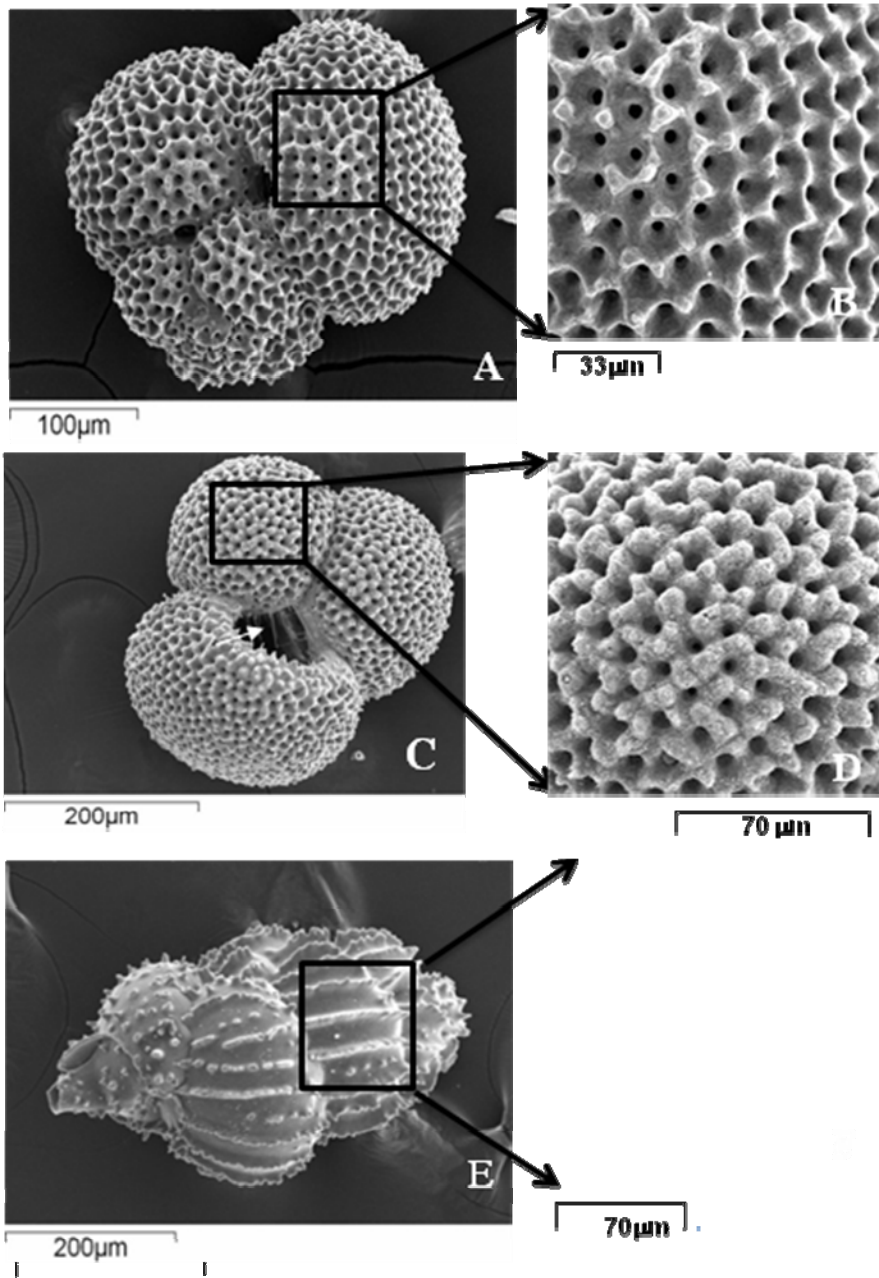


Fig.3

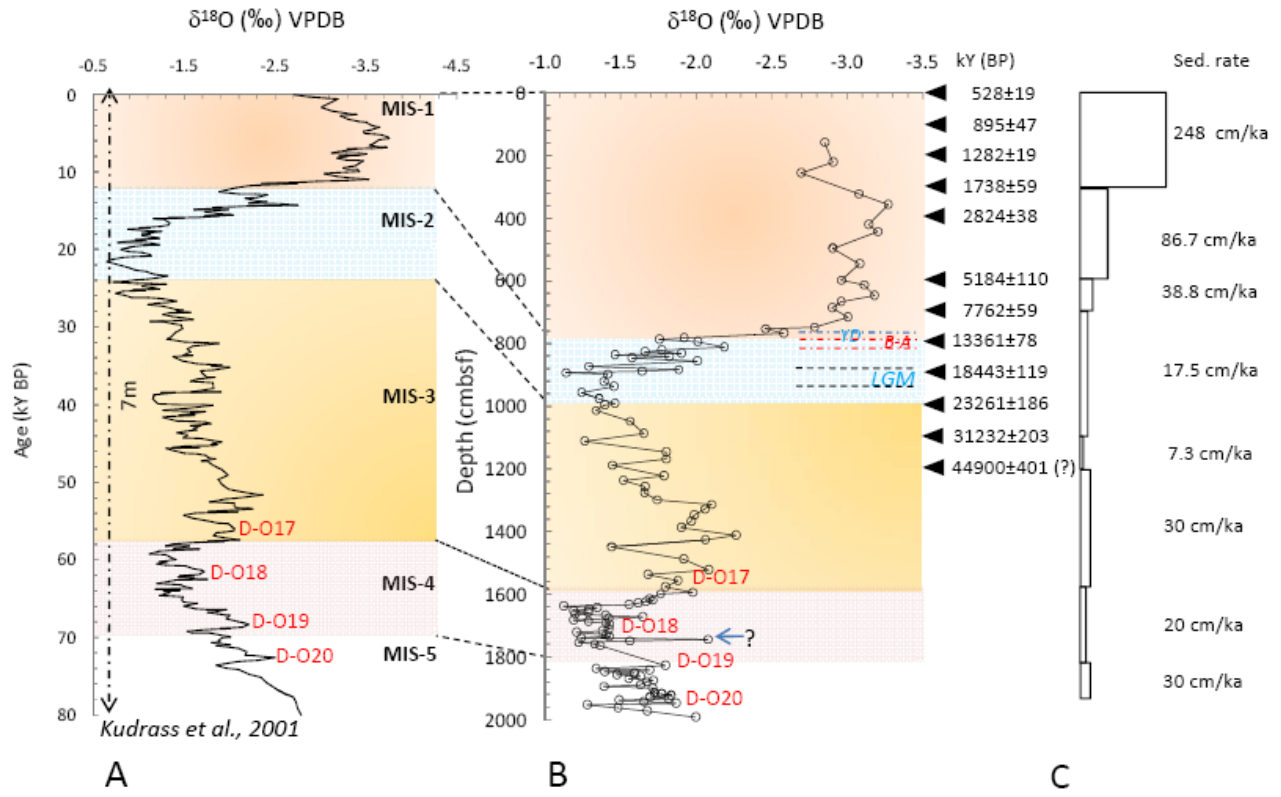


Fig.4

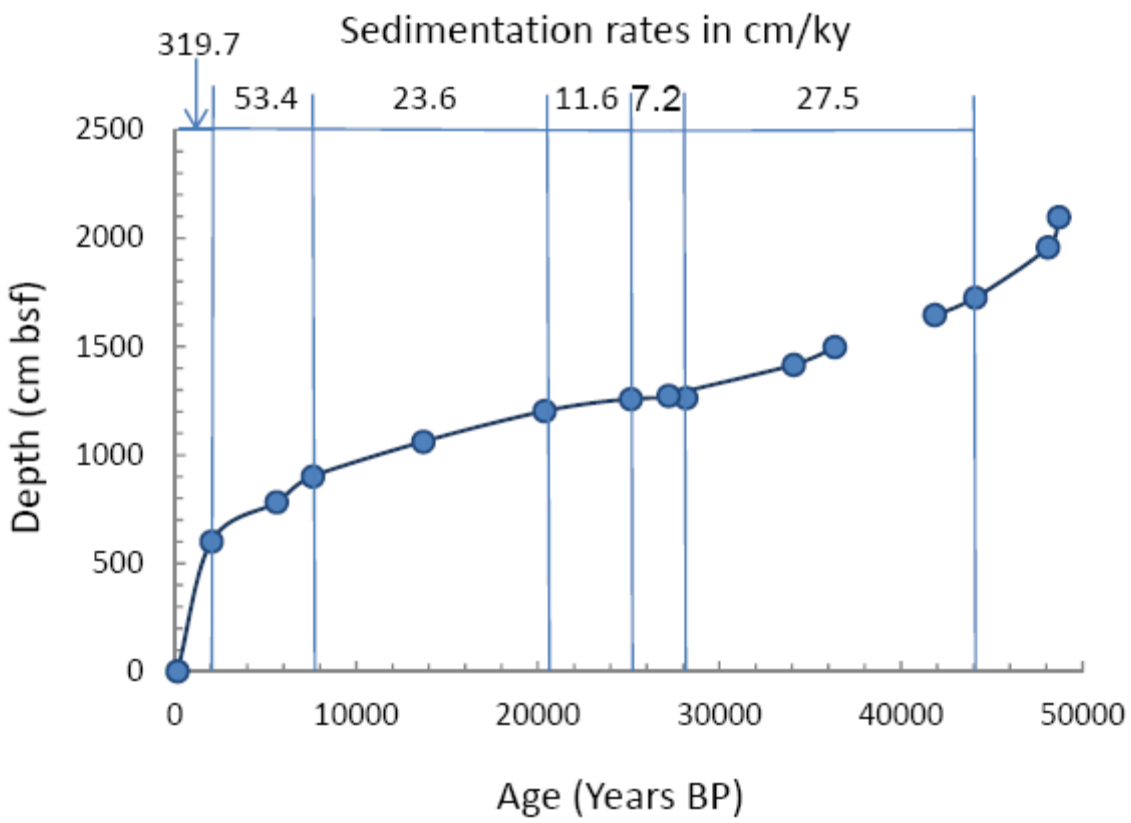


Fig.5

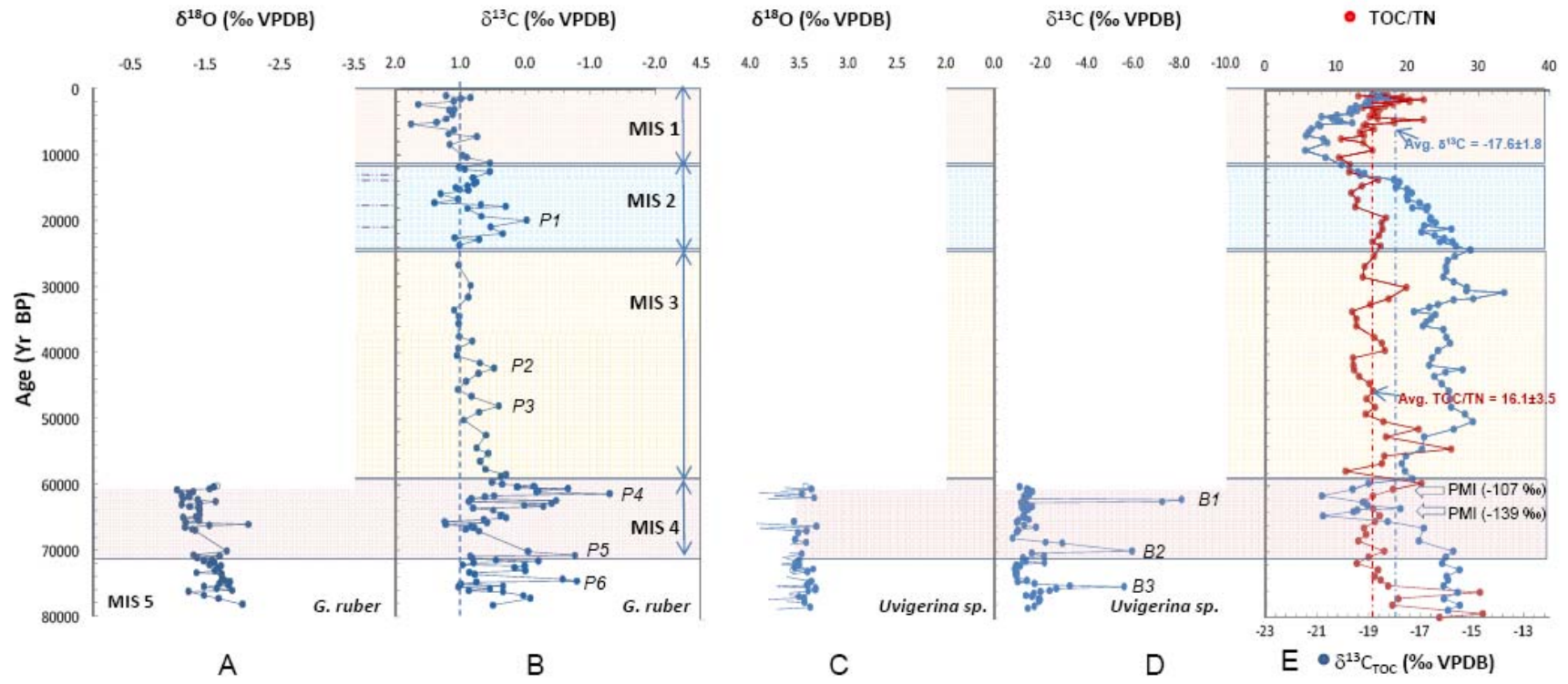


Fig.6

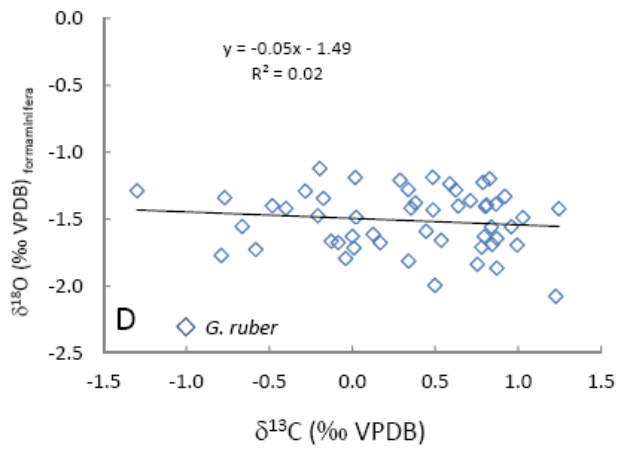
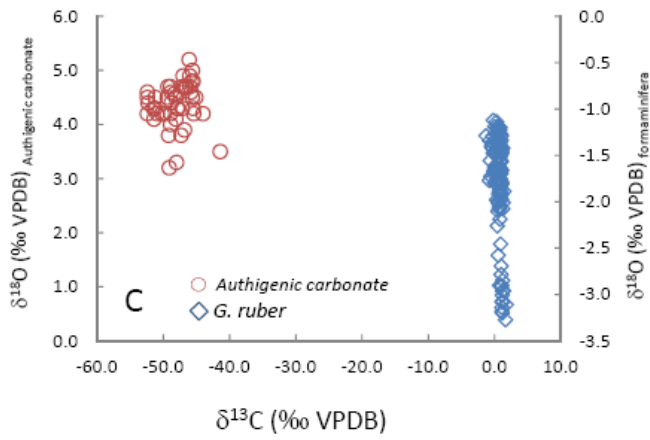
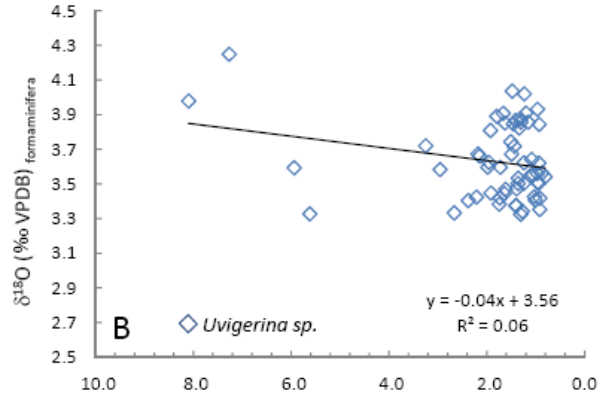
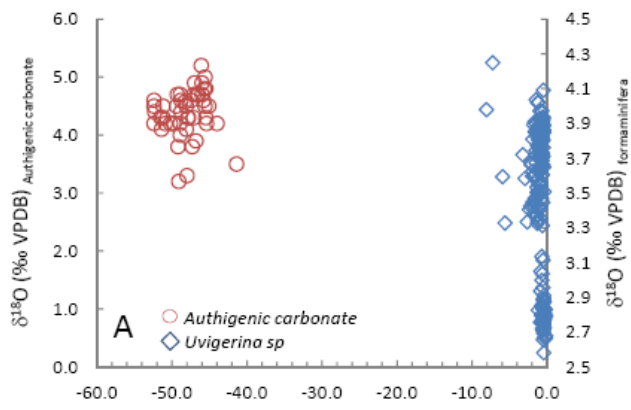


Fig. 7

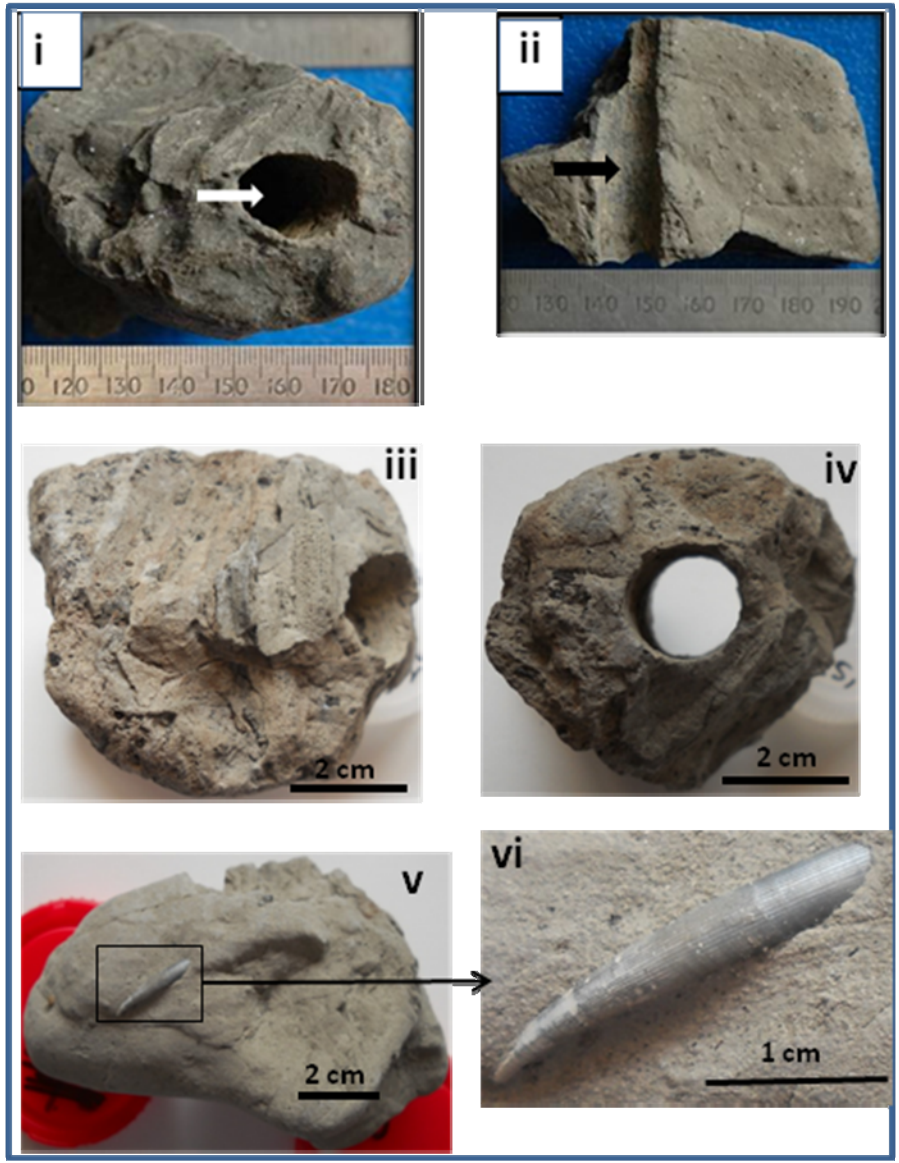


Fig.8

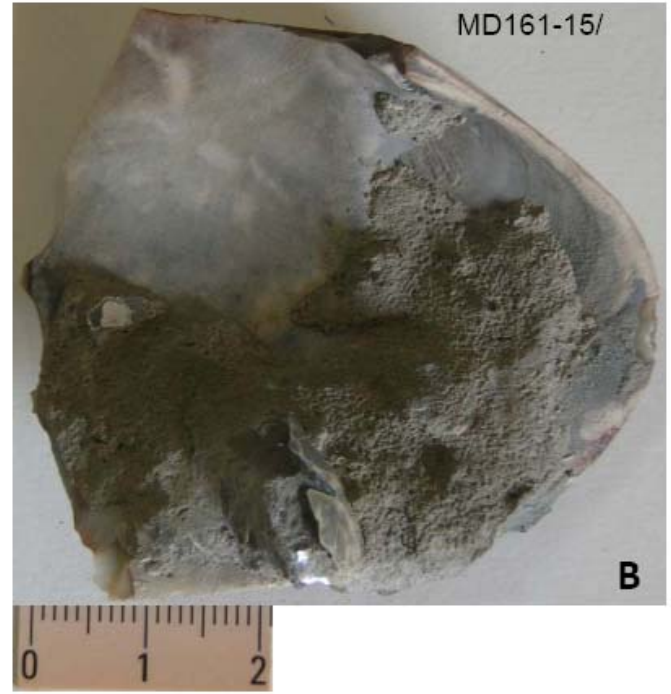
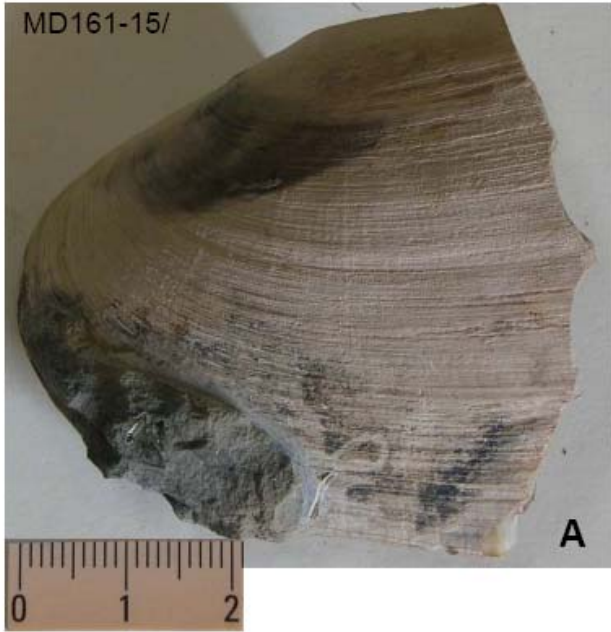


Fig.9

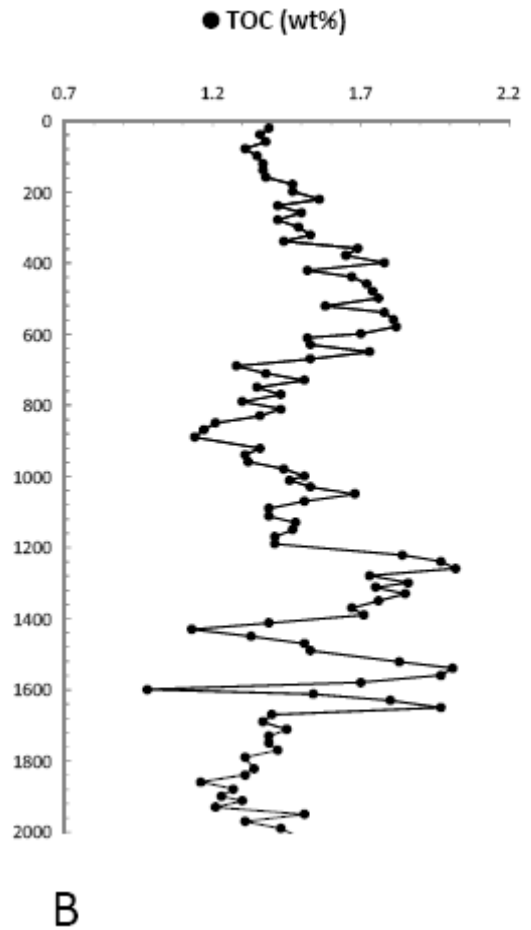
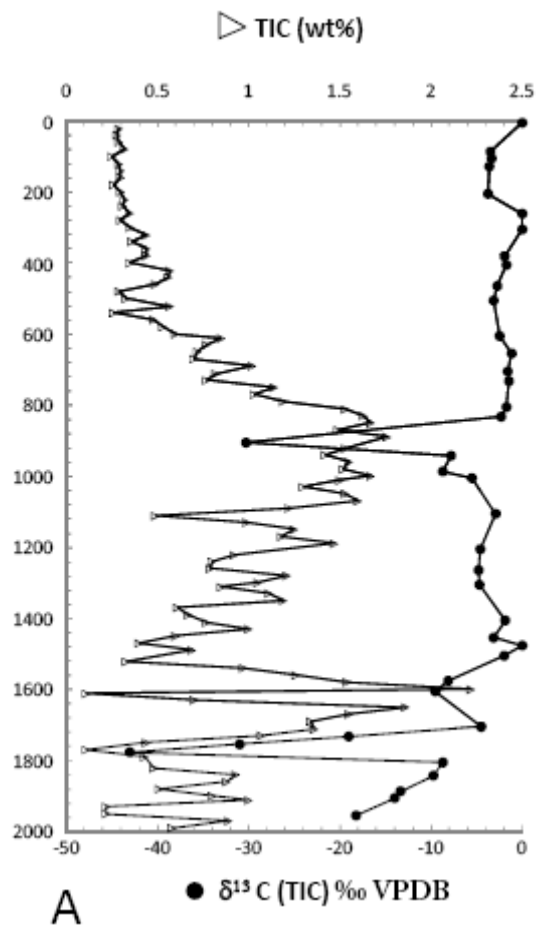
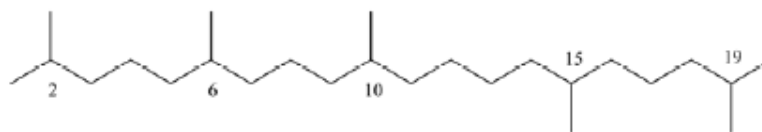


Fig.10

Structure of PMI

Molecular formula: C₂₅H₅₂

Molecular weight: 352



2,6,10,15,19-pentamethylicosane

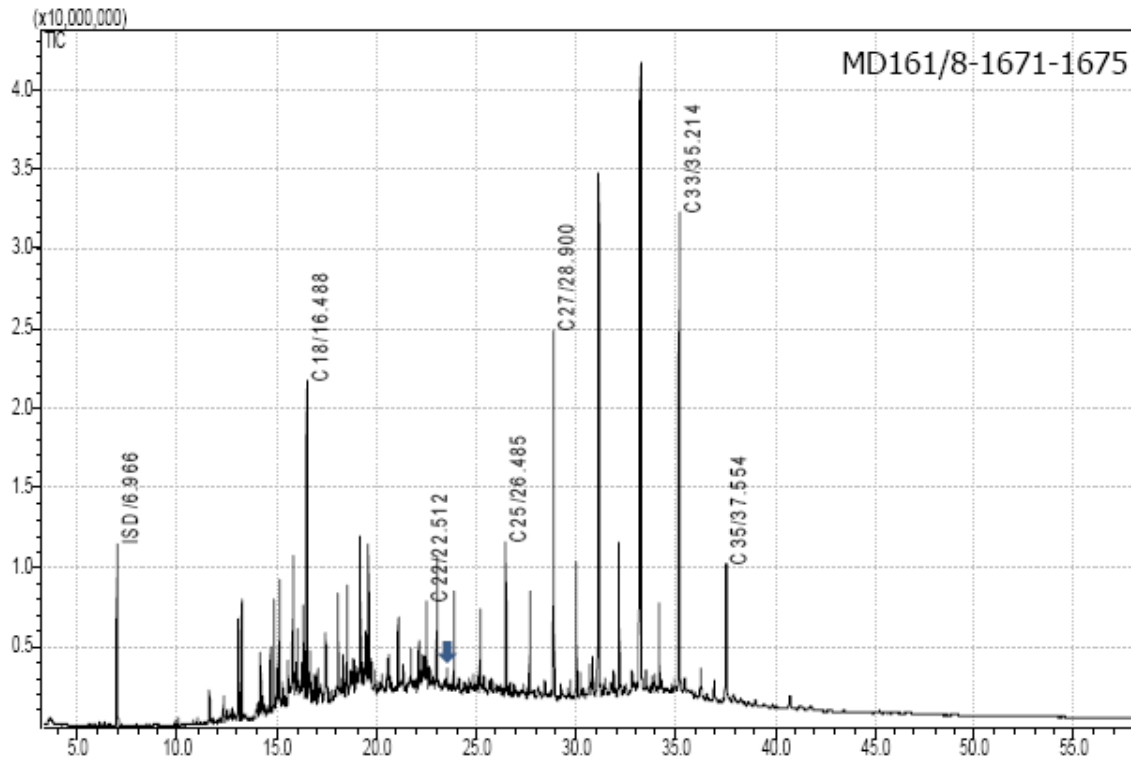
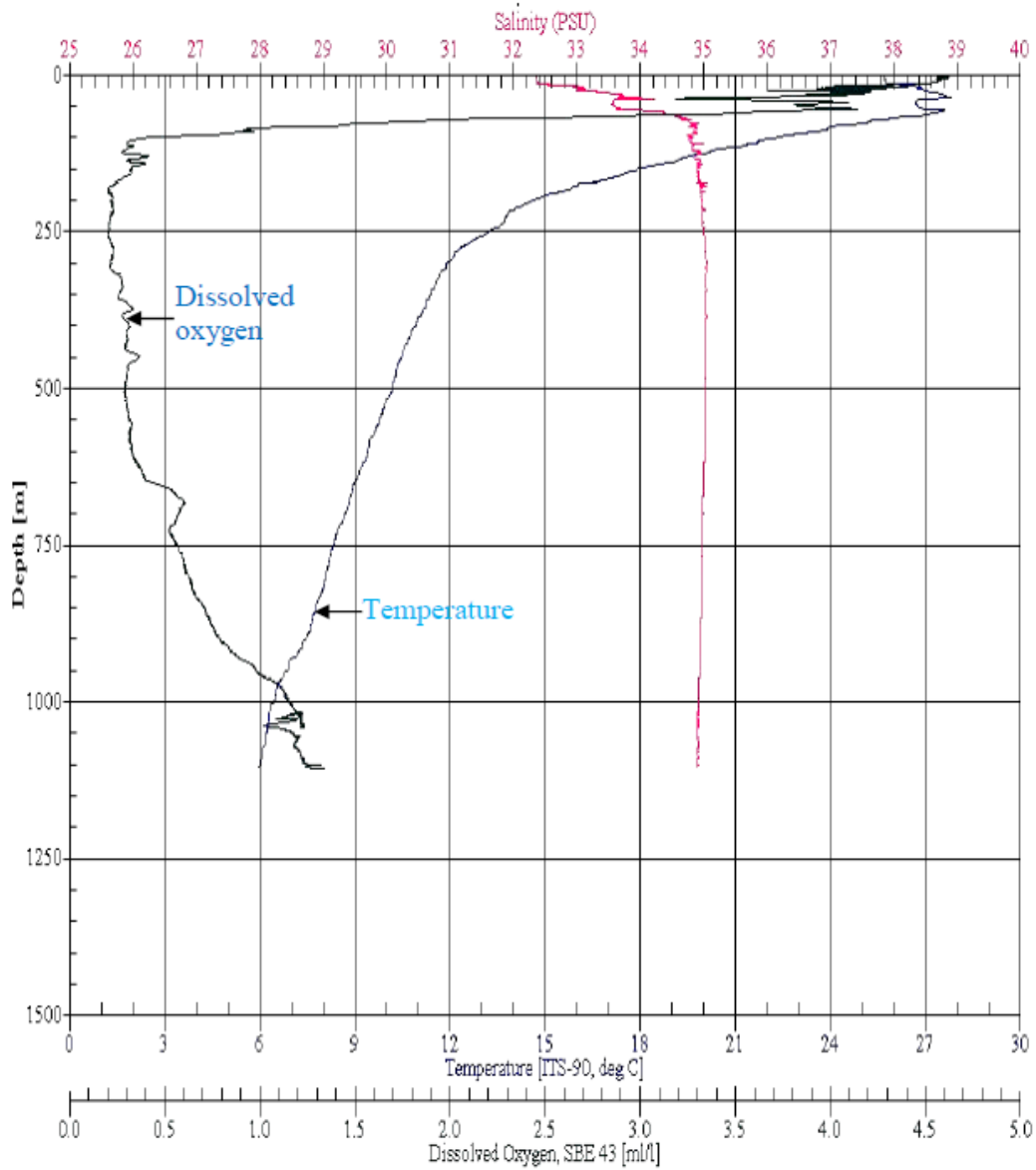


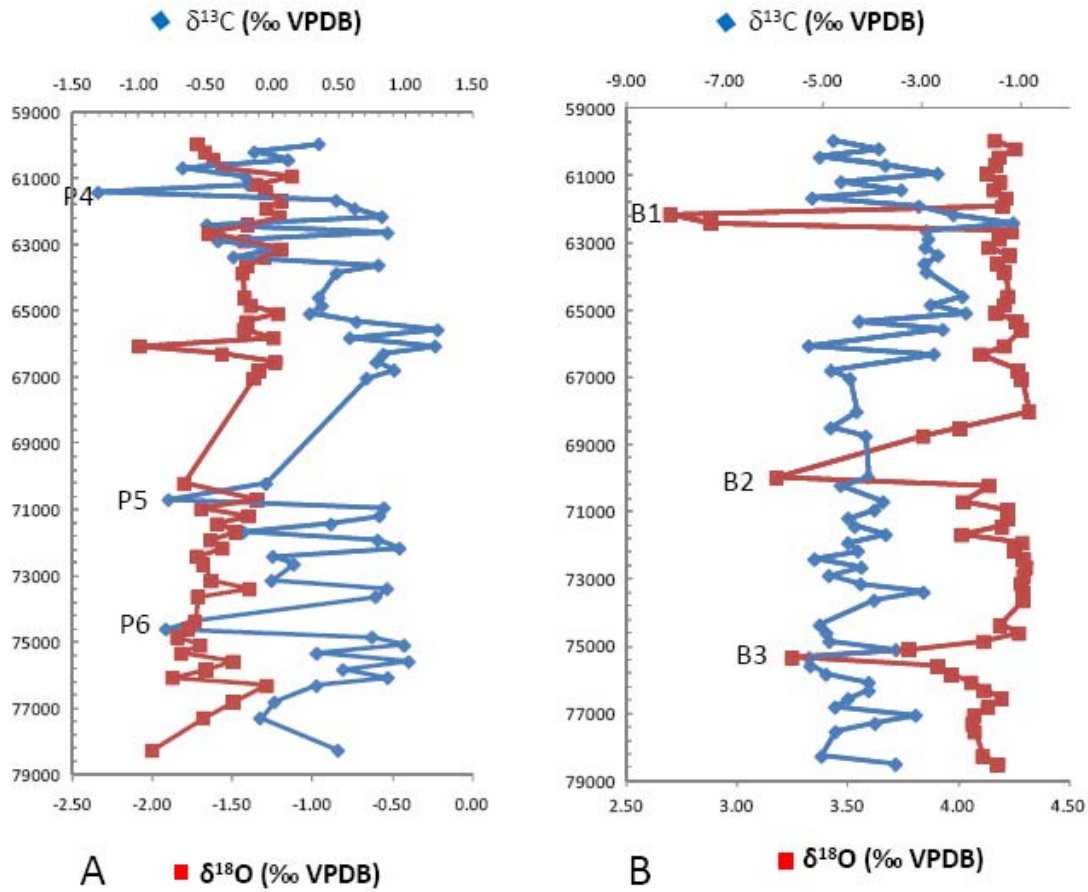
Fig.11



Supplementary Fig-1. Temperature, salinity and dissolved oxygen profiles of sea water column near site MD161-8.

G. ruber

Uvigerina sp.



Suppl. Figure-2. Blowup of the benthic and planktic foraminifera carbon and oxygen isotope profiles within the age bracket (59000-79000 y BP).

Table TS 1. Carbon and oxygen stable isotope ratios of planktic foraminifera (*G. ruber*) of MD161-8.

Mean Depth (Cmbsf)	Age (y)	$\delta^{18}\text{C}$ (‰VPDB)	$\delta^{13}\text{O}$ (‰VPDB)
157.5	1097.7	1.22	-2.85
222.5	1375.5	0.85	-2.90
257.5	1523.3	0.99	-2.69
322.5	1907.4	1.10	-3.08
357.5	2311.0	1.65	-3.27
422.5	3060.4	1.09	-3.14
442.5	3291.0	1.17	-3.20
497.5	3925.2	1.12	-2.91
547.5	4501.7	1.22	-3.08
597.5	5078.2	1.37	-2.96
612.5	5364.3	1.75	-3.11
647.5	6266.6	1.09	-3.18
667.5	6782.2	1.17	-2.96
687.5	7297.8	0.75	-2.90
717.5	8485.5	1.16	-3.01
747.5	10087.0	0.97	-2.79
752.5	10351.0	0.91	-2.46
767.5	11155.9	0.54	-2.58
782.5	11957.2	1.02	-1.92
787.5	12224.3	0.92	-1.76
794.5	12598.2	0.55	-2.01
812.5	13559.8	0.81	-2.19
822.5	14095.0	0.76	-1.77
827.5	14361.1	0.79	-1.66
832.5	14629.2	0.88	-1.90
837.5	14895.3	1.07	-1.47
842.5	15163.4	1.01	-1.82
847.5	15429.5	0.88	-1.57
857.5	15964.7	1.30	-2.01
872.5	16765.0	1.04	-1.29
882.5	17300.2	1.40	-1.89
887.5	17566.3	0.68	-1.64
892.5	17834.4	0.30	-1.14
897.5	18100.5	0.88	-1.41
922.5	19267.1	0.67	-1.39
937.5	19985.9	-0.03	-1.45
957.5	20949.9	0.53	-1.25
977.5	21910.4	0.35	-1.36
992.5	22624.7	1.09	-1.47

997.5	22869.0	0.72	-1.39
1012.5	23645.6	1.01	-1.34
1047.5	26650.9	1.03	-1.57
1087.5	29765.3	0.84	-1.66
1112.5	31607.6	0.88	-1.26
1147.5	33485.4	1.09	-1.80
1167.5	34558.4	1.02	-1.80
1187.5	35631.4	1.03	-1.44
1222.5	37509.1	1.02	-1.78
1237.5	38313.9	0.81	-1.52
1257.5	39386.9	1.02	-1.66
1277.5	40459.9	1.05	-1.66
1297.5	41532.9	0.69	-1.74
1312.5	42362.0	0.48	-2.10
1327.5	43229.9	0.73	-2.05
1347.5	44383.9	0.91	-1.99
1367.5	45536.9	1.03	-1.97
1387.5	46689.9	0.83	-1.90
1412.5	48137.1	0.40	-2.26
1427.5	49007.9	0.71	-2.06
1447.5	50167.9	0.94	-1.44
1487.5	52469.0	0.61	-1.91
1522.5	54506.6	0.74	-2.08
1537.5	55358.6	0.57	-1.68
1557.5	56519.7	0.70	-1.88
1577.5	57669.3	0.62	-1.79
1592.5	58535.5	0.30	-1.98
1597.5	58820.5	0.37	-1.77
1612.5	59720.0	0.51	-1.69
1617.5	59964.0	0.36	-1.71
1622.5	60208.0	-0.13	-1.66
1627.5	60452.0	0.12	-1.61
1632.5	60696.0	-0.66	-1.55
1637.5	60940.0	-0.20	-1.12
1642.5	61184.0	-0.17	-1.34
1647.5	61428.0	-1.30	-1.29
1652.5	61672.0	0.48	-1.19
1657.5	61916.0	0.62	-1.28
1662.5	62160.0	0.83	-1.20
1667.5	62404.0	-0.48	-1.40
1672.5	62648.0	0.87	-1.64
1677.5	62892.0	-0.40	-1.42
1682.5	63136.0	0.02	-1.19

1687.5	63380.0	-0.28	-1.29
1692.5	63624.0	0.80	-1.41
1697.5	63868.0	0.49	-1.43
1712.5	64600.0	0.35	-1.42
1717.5	64844.0	0.38	-1.38
1722.5	65088.0	0.29	-1.21
1727.5	65332.0	0.64	-1.40
1732.5	65576.0	1.25	-1.42
1737.5	65820.0	0.59	-1.24
1742.5	66064.0	1.23	-2.08
1747.5	66308.0	0.84	-1.56
1752.5	66552.0	0.79	-1.23
1757.5	66796.0	0.92	-1.33
1762.5	67040.0	0.71	-1.36
1827.5	70212.0	-0.04	-1.79
1837.5	70700.0	-0.77	-1.34
1842.5	70944.0	0.84	-1.69
1847.5	71188.0	0.81	-1.39
1852.5	71432.0	0.45	-1.59
1857.5	71676.0	-0.21	-1.47
1862.5	71920.0	0.80	-1.63
1867.5	72164.0	0.96	-1.56
1872.5	72408.0	0.01	-1.72
1877.5	72652.0	0.17	-1.68
1887.5	73140.0	0.00	-1.63
1892.5	73384.0	0.87	-1.39
1897.5	73628.0	0.78	-1.71
1912.5	74360.0	-0.58	-1.73
1917.5	74604.0	-0.79	-1.77
1922.5	74848.0	0.75	-1.84
1927.5	75092.0	0.99	-1.69
1932.5	75336.0	0.34	-1.81
1937.5	75580.0	1.03	-1.49
1942.5	75824.0	0.54	-1.66
1947.5	76068.0	0.87	-1.87
1952.5	76312.0	0.34	-1.28
1962.5	76800.0	0.02	-1.49
1972.5	77288.0	-0.09	-1.68
1992.5	78264.0	0.50	-1.99

Table TS 2. Carbon and oxygen stable isotope ratios of benthic foraminifera (*Uvigerina* sp.) of MD161-8.

Mean Depth (cmbsf)	Age (y)	$\delta^{18}\text{O}$ (‰VPDB)	$\delta^{13}\text{C}$ (‰VPDB)
32.5	627.7	2.79	-0.49
42.5	665.3	2.75	-0.46
52.5	702.9	2.89	-0.54
127.5	984.9	2.66	-0.53
147.5	1060.1	2.89	-0.47
222.5	1376.0	2.67	-0.31
227.5	1388.6	2.67	-0.23
252.5	1500.9	2.58	-0.46
257.5	1523.0	2.68	-0.18
327.5	1979.7	2.69	-0.45
337.5	2088.3	2.72	-0.62
347.5	2196.9	2.81	-0.35
357.5	2311.0	2.80	-0.50
362.5	2359.8	2.91	-0.46
367.5	2414.1	2.78	-0.54
372.5	2468.4	2.71	-0.52
377.5	2522.7	2.79	-0.43
382.5	2577.0	2.80	-0.49
387.5	2631.3	2.77	-0.35
392.5	2685.6	2.77	-0.54
422.5	3060.4	2.96	-0.56
437.5	3221.3	2.72	-0.62
442.5	3291.0	2.83	-0.25
457.5	3453.5	2.72	-0.45
472.5	3628.4	2.83	-0.34
487.5	3803.3	2.73	-0.38
497.5	3925.2	2.75	-0.46
522.5	4211.4	3.11	-0.55
527.5	4269.7	2.79	-0.19
537.5	4386.3	2.76	-0.47
552.5	4562.2	2.78	-0.57
557.5	4619.5	2.71	-0.56
567.5	4737.1	2.85	-0.51
577.5	4853.7	2.76	-0.67
587.5	4969.3	2.88	-0.42
597.5	5078.2	2.79	-0.50

612.5	5364.3	2.88	-0.41
622.5	5622.1	2.83	-0.56
627.5	5751.0	2.84	-0.65
637.5	6008.8	2.84	-0.51
647.5	6266.6	3.14	-0.71
652.5	6395.5	2.76	-0.51
657.5	6524.4	2.83	-1.19
667.5	6782.2	2.76	-0.90
672.5	6911.1	2.80	-0.78
677.5	7040.0	2.86	-0.60
687.5	7297.8	2.84	-0.54
692.5	7426.7	2.80	-0.71
697.5	7555.6	2.85	-0.75
722.5	8685.3	3.00	-0.70
727.5	8961.3	2.94	-0.88
737.5	9512.9	3.05	-0.87
742.5	9791.0	3.47	-0.74
747.5	10087.0	3.04	-0.65
752.5	10351.0	3.31	-0.65
757.5	10619.1	3.88	-0.69
782.5	11957.2	3.85	-0.58
787.5	12224.3	3.69	-0.69
797.5	12834.7	3.51	-0.42
812.5	13559.8	3.72	-0.62
822.5	14095.0	3.89	-0.72
827.5	14361.1	3.73	-0.76
832.5	14629.2	3.85	-0.48
837.5	14895.3	3.71	-0.56
847.5	15429.5	3.65	-0.45
852.5	15695.6	3.80	-0.65
857.5	15964.7	3.65	-0.69
862.5	16228.8	3.70	-0.66
867.5	16490.2	4.09	-0.51
872.5	16765.0	3.93	-0.51
882.5	17300.2	3.61	-0.64
887.5	17566.3	3.90	-0.61
892.5	17834.4	3.45	-0.59
897.5	18100.5	3.76	-0.52
922.5	19267.1	3.89	-0.44

927.5	19502.3	3.97	-0.70
937.5	19985.9	3.80	-0.55
947.5	20457.7	3.92	-0.54
957.5	20949.9	4.02	-1.22
967.5	21423.8	3.94	-0.58
977.5	21910.4	3.91	-0.77
987.5	22382.5	3.86	-0.45
997.5	22869.0	3.66	-0.75
1012.5	23645.6	3.87	-0.72
1017.5	24133.0	3.83	-0.79
1027.5	24952.5	3.66	-0.57
1037.5	25754.8	3.88	-0.98
1047.5	26650.9	3.86	-0.54
1057.5	27370.3	3.81	-0.71
1067.5	28177.4	3.81	-0.60
1077.5	28981.5	3.91	-0.63
1087.5	29765.3	3.86	-0.53
1097.5	30581.8	3.88	-0.80
1112.5	31607.6	3.83	-0.68
1117.5	31875.9	3.73	-0.67
1127.5	32412.4	3.81	-0.74
1137.5	32846.5	3.80	-0.83
1147.5	33485.4	3.75	-1.03
1157.5	34003.2	3.79	-0.94
1167.5	34558.4	3.71	-0.83
1177.5	35072.9	3.82	-0.68
1187.5	35631.4	3.35	-1.16
1222.5	37509.1	3.71	-0.89
1237.5	38313.9	3.92	-0.72
1257.5	39386.9	3.72	-0.92
1277.5	40459.9	3.69	-0.87
1297.5	41532.9	3.77	-0.90
1312.5	42362.0	3.83	-0.89
1327.5	43229.9	3.73	-0.87
1347.5	44383.9	3.74	-0.89
1367.5	45536.9	3.88	-1.02
1387.5	46689.9	3.86	-0.85
1412.5	48137.1	3.84	-1.01
1427.5	49007.9	3.77	-1.17

1447.5	50167.9	3.89	-0.84
1467.5	51308.8	3.66	-0.92
1537.5	55358.6	3.89	-0.69
1557.5	56519.7	3.77	-1.29
1577.5	57669.3	3.97	-0.97
1592.5	58535.5	3.80	-1.14
1597.5	58820.5	3.81	-1.00
1612.5	59720.0	3.58	-1.18
1617.5	59964.0	3.44	-1.50
1622.5	60208.0	3.64	-1.08
1627.5	60452.0	3.38	-1.41
1632.5	60696.0	3.67	-1.49
1637.5	60940.0	3.91	-1.66
1642.5	61184.0	3.47	-1.39
1647.5	61428.0	3.74	-1.51
1652.5	61672.0	3.34	-1.27
1657.5	61916.0	3.82	-1.34
1662.5	62160.0	3.98	-8.09
1667.5	62404.0	4.25	-7.27
1672.5	62648.0	3.86	-1.15
1677.5	62892.0	3.87	-1.41
1682.5	63136.0	3.85	-1.63
1687.5	63380.0	3.91	-1.20
1692.5	63624.0	3.85	-1.46
1697.5	63868.0	3.86	-1.30
1712.5	64600.0	4.02	-1.23
1717.5	64844.0	3.88	-1.31
1722.5	65088.0	4.04	-1.48
1727.5	65332.0	3.55	-1.06
1732.5	65576.0	3.93	-0.96
1742.5	66064.0	3.33	-1.31
1747.5	66308.0	3.89	-1.80
1757.5	66796.0	3.43	-1.03
1762.5	67040.0	3.51	-0.96
1782.5	68016.0	3.54	-0.81
1792.5	68504.0	3.42	-2.21
1797.5	68748.0	3.58	-2.96
1822.5	69968.0	3.59	-5.94
1827.5	70212.0	3.47	-1.62

1837.5	70700.0	3.66	-2.15
1842.5	70944.0	3.62	-1.24
1847.5	71188.0	3.50	-1.24
1852.5	71432.0	3.53	-1.36
1857.5	71676.0	3.67	-2.18
1862.5	71920.0	3.50	-0.94
1867.5	72164.0	3.55	-1.11
1872.5	72408.0	3.35	-0.92
1877.5	72652.0	3.56	-0.88
1882.5	72896.0	3.42	-0.92
1887.5	73140.0	3.56	-0.97
1892.5	73384.0	3.84	-0.93
1897.5	73628.0	3.62	-0.94
1912.5	74360.0	3.38	-1.40
1917.5	74604.0	3.41	-1.01
1922.5	74848.0	3.42	-1.73
1927.5	75092.0	3.72	-3.25
1932.5	75336.0	3.33	-5.62
1937.5	75580.0	3.33	-2.67
1942.5	75824.0	3.40	-2.38
1947.5	76068.0	3.60	-1.98
1952.5	76312.0	3.60	-1.72
1957.5	76556.0	3.50	-1.36
1962.5	76800.0	3.45	-1.64
1967.5	77044.0	3.81	-1.92
1972.5	77288.0	3.63	-1.96
1977.5	77532.0	3.45	-1.92
1992.5	78264.0	3.38	-1.75
1997.5	78508.0	3.72	-1.44

Supplementary Table- 3: Mineralogy and $\delta^{13}\text{C}$ values of authigenic carbonate samples from MD161-15

Sample depth(cm)	Carbonate Mineralogy by XRD	$\delta^{13}\text{C}$ (‰ VPDB)	MgCO ₃ (mole %)
2711	High Mg calcite	-47.3	6.3
2897.5	High Mg calcite	-50.2	11.42
2902.5	High Mg calcite	-46.8	12.5
2920	High Mg calcite	-47.9	12.8

Suppl. Table-4. Total organic carbon content (TOC wt %), $\delta^{13}\text{C}_{\text{TOC}}$ (‰ VPDB) and Total inorganic carbon content (TIC wt%) in MD161-8.

Depth (cmbsf)	TOC %	TIC %	TN %	Depth (cmbsf)	$\delta^{13}\text{C}$
21	1.39	0.29	0.09	21	-18.9
39	1.36	0.28	0.08	39	-18.5
59	1.38	0.29	0.08	59	-18.7
79	1.31	0.32	0.10	79	-18.5
99	1.35	0.25	0.07	99	-18.5
121	1.37	0.29	0.08	121	-18.7
139	1.37	0.30	0.08	139	-18.2
159	1.38	0.30	0.08	159	-18.2
179	1.47	0.26	0.08	179	-18.2
199	1.47	0.30	0.08	199	-18.2
221	1.56	0.32	0.07	221	-19.0
239	1.42	0.31	0.07	239	-18.8
259	1.50	0.35	0.08	259	-19.0
279	1.42	0.30	0.07	279	-18.9
299	1.49	0.35	0.10	299	-18.9
321	1.53	0.44	0.09	321	-19.1
339	1.44	0.36	0.08	339	-19.0
359	1.69	0.44	0.10	359	-19.5
379	1.65	0.44	0.12	379	-19.5
399	1.78	0.35	0.11	399	-19.7
421	1.52	0.57	0.10	421	-19.4
439	1.67	0.56	0.11	439	-19.7
459	1.72	0.49	0.11	459	-19.7
479	1.74	0.29	0.11	479	-20.2
499	1.76	0.33	0.12	499	-20.8
521	1.58	0.57	0.10	521	-20.4
539	1.78	0.26	0.08	539	-20.2
559	1.81	0.48	0.10	559	-20.1
579	1.82	0.53	0.10	579	-19.6
599	1.70	0.60	0.12	599	-20.9
611	1.52	0.85	0.11	611	-20.9
629	1.53	0.77	0.10	629	-21.2
649	1.73	0.72	0.13	649	-21.3

669	1.53	0.70	0.11	669	-21.4
689	1.28	1.02	0.12	689	-20.7
711	1.38	0.82	0.10	711	-20.6
729	1.51	0.77	0.10	729	-21.5
749	1.35	1.14	0.13	749	-20.7
769	1.43	1.03	0.12	769	-20.1
789	1.30	1.19	0.11	789	-19.4
811	1.43	1.53	0.09	793	-19.2
829	1.36	1.63	0.10	798	-19.3
849	1.21	1.67	0.10	811	-18.0
869	1.17	1.49	0.09	818	-17.8
889	1.14	1.76	0.09	829	-17.9
921	1.36	1.53	0.08	833	-17.9
939	1.31	1.42	0.08	838	-17.5
959	1.32	1.55	0.08	849	-17.3
979	1.44	1.52	0.09	858	-17.5
999	1.51	1.67	0.10	869	-17.5
1011	1.46	1.50	0.09	878	-17.0
1029	1.53	1.30	0.10	889	-16.7
1049	1.68	1.53	0.12	893	-17.3
1069	1.51	1.60	0.11	898	-16.8
1089	1.39	1.22	0.07	921	-16.6
1111	1.39	0.49	0.08	928	-16.6
1129	1.48	0.99	0.10	939	-16.4
1149	1.47	1.25	0.12	948	-16.9
1169	1.41	1.18	0.11	959	-15.8
1189	1.41	1.47	0.11	968	-17.0
1221	1.84	0.92	0.12	979	-16.4
1239	1.97	0.80	0.12	988	-16.1
1259	2.02	0.79	0.12	998	-15.8
1279	1.73	1.21	0.14	999	-16.2
1299	1.86	1.05	0.15	1011	-15.6
1311	1.75	0.85	0.14	1018	-15.1
1329	1.85	1.11	0.14	1029	-15.7
1349	1.76	1.19	0.12	1038	-15.9
1369	1.67	0.61	0.11	1049	-16.0
1389	1.71	0.67	0.12	1058	-16.0
1411	1.39	0.77	0.09	1069	-16.1
1429	1.13	1.00	0.08	1078	-15.7

1449	1.33	0.60	0.08	1089	-15.2
1469	1.51	0.40	0.07	1093	-15.2
1489	1.53	0.69	0.09	1098	-13.8
1521	1.83	0.33	0.07	1111	-15.0
1539	2.01	0.97	0.12	1118	-15.7
1559	1.97	1.26	0.12	1129	-16.3
1579	1.70	1.54	0.15	1138	-16.7
1599	0.98	2.22	0.16	1149	-17.2
1611	1.54	0.11	0.07	1158	-16.4
1629	1.80	0.70	0.10	1169	-16.6
1649	1.97	1.86	0.13	1178	-16.8
1669	1.40	1.55	0.10	1189	-16.9
1689	1.37	1.34	0.09	1198	-16.1
1711	1.45	1.36	0.09	1221	-16.0
1729	1.39	1.07	0.09	1239	-15.9
1749	1.39	0.44	0.10	1259	-16.3
1769	1.42	0.11	0.10	1279	-16.5
1789	1.31	0.43	0.10	1299	-16.7
1821	1.34	0.48	0.08	1311	-15.4
1839	1.31	0.93	0.09	1318	-16.0
1859	1.16	0.88	0.09	1329	-16.5
1879	1.27	0.51	0.08	1349	-16.2
1899	1.23	0.80	0.08	1369	-15.9
1911	1.30	1.00	0.08	1389	-15.9
1929	1.21	0.22	0.07	1411	-15.8
1949	1.51	0.22	0.05	1429	-15.3
1969	1.31	0.89	0.07	1449	-15.0
1989	1.43	0.58	0.08	1469	-15.7
2029	1.53	0.23	0.05	1489	-16.9
				1521	-16.9
				1539	-17.6
				1559	-17.7
				1579	-17.6
				1599	-17.3
				1611	-19.0
				1629	-19.6
				1649	-20.8
				1669	-19.2
				1679	-19.0

1689	-17.8
1693	-19.4
1698	-19.6
1711	-20.8
1729	-18.3
1749	-16.9
1789	-17.1
1821	-15.7
1839	-16.0
1859	-16.2
1879	-15.5
1899	-16.0
1911	-15.9
1929	-16.1
1949	-15.6
1969	-16.1
1989	-15.5
2011	-15.9
